Investigating the relationship between volume transport and sea surface height in the Agulhas Current System

Physical Oceanography

Estee Vermeulen

Dr. Juliet Hermes
Dr. Björn Backeberg
Dr. Shane Elipot
Assoc. Prof Marcello Vichi

Dissertation submitted in fulfilment of the requirements for the degree in Masters of Science (MSc.)

Department of Oceanography, University of Cape Town

August 2017

Declaration of Authorship

I, **Estee Vermeulen**, declare that the contents of this dissertation titled, "Investigating the relationship between volume transport and sea surface height in the Agulhas Current System" represents my own work, aided by my supervisors.

- This dissertation has not previously been submitted for academic examination towards any qualification.
- I have used the Harvard convention for citation and referencing, therefore each significant contribution to, and quotation in this dissertation from the work of others has been attributed, and has been cited and referenced.
- This dissertation represents my own opinions and not necessarily those of the University of Cape Town.

Signed: Signed by candidate Date: 20/11/2017

Signature Removed

UNIVERSITY OF CAPE TOWN

Abstract

Faculty of Science

Department of Oceanography

Master of Science

Investigating the relationship between volume transport and sea surface height in the Agulhas Current System

by Estee Ann Vermeulen

The relationship between the volume transport of the Agulhas Current at 34°S (the position of the Agulhas Current Time-series array) and the gradient of sea surface height across the current is investigated using a regional Hybrid Coordinate Ocean Model. Previous studies have suggested a high correlation between SSH slope and Agulhas Current transport and, based on 3 years of *in situ* measurements, a transport proxy between along-track satellite data and *in situ* data was developed. The purpose of this modelling study was to re-create the Agulhas Current transport proxy in a virtual modelling environment, to test the validity of the underlying assumption on which the satellite-altimeter proxy was based. The Agulhas transport proxy assumed nine, constant linear relationships between SSH slope and integrated transport per unit distance over the 22-year transport time-series, based on the 3-year sampling period and a constant vertical stratification. The 34-year regional-hindcast from HYCOM provided the means to test the sensitivity of the transport proxy to vertical changes in the current and the length scale of observations used to build a constant, linear relationship between transport and SSH slope. During the investigation it was found that HYCOM contained exaggerated levels of offshore variability. This resulted in stronger correlations for the inshore linear regression models with a decreasing trend moving offshore. Based on the overall performance of the 34-year transport proxies it was concluded that the proxy was more capable of estimating the net transport of the Agulhas Current across the array instead of only the southwest transport component. Therefore, transport estimates inshore were more accurate than the transport estimates offshore, when the current is in a meandering state, and the poorer performance of the southwest transport proxy, specifically developed to capture the transport during offshore meander events, was less capable of estimating an accurate transport estimate. Results showed that calculating the proxy over longer time periods did not significantly improve the skill of the Agulhas transport proxy, suggesting the 3-years was a sufficient time-period used to develop the transport proxy in HYCOM. This study motivates the need to improve long-term monitoring methods, where the usage of numerical ocean models could help understand the sensitivities and limitations involved in the development of transport proxies in future.

Acknowledgements

I wish to thank my supervisors Dr. Juliet Hermes, Dr. Björn Backeberg, Dr. Shane Elipot and lastly Associate Professor Marcello Vichi for the valuable guidance provided throughout my dissertation. I would also like to acknowledge Dr. Knut Arild Liæster, for all his help provided, whilst working together at the Nansen Center in Bergen. Having completed a MSc. in Physical Oceanography has left me feeling very proud and ready to take on my next milestone as a marine scientist.

I have gained a considerable amount of skills throughout the past two years. I was given the opportunity to partake in an exchange semester at the University of Bergen, Norway, which for me, was the best experience during of my MSc. Working amongst senior scientists and being part of the ocean modelling group at the Nansen Environmental Remote Sensing Centre (NERSC) in Bergen allowed me to learn a great deal about the intricacies involved in ocean modelling, and allowed me to advance my programming knowledge. I also attended two courses at the Geophysical Institute; Dynamics of the Ocean and Atmosphere and Energy Studies, which I thoroughly enjoyed and obtained distinctions in both examinations. For this, I have to thank Björn, Marcello and Sharon Bosma, who assisted me with the funding provided by the bilateral South Africa Norway SANCOOP SCAMPI project as well as Knut Liæster, Annette Samualson and Johnny Johansson for making me feel welcome at NERSC.

Thank you Björn and Juliet for all the help, you were always there whenever I needed assistance. Thanks Bjorn for providing the HYCOM data for this project and Juliet for introducing me to many scientists in the field of marine science in South Africa. Marcello, your door was always open to me and I really enjoyed tutoring the undergraduate students in your Ocean Dynamics course.

I gratefully acknowledge Dr. Shane Elipot and Professor Lisa Beal from the Rosenstiel School of Marine and Atmospheric Science (RSMAS), University of Miami, for granting us permission to replicate the Agulhas transport proxy methods. Shane, you have taught me a great deal about statistical analysis throughout my project and through your data analysis course at the environmental time-series analysis conference, in Tromsø. I'm looking forward to working with you in the future.

I would lastly like to acknowledge the National Research Foundation (NRF) for the scarce skills masters scholarship offered to fund my research. Opinions expressed in this dissertation and the conclusions arrived at are not necessarily to be attributed the NRF.

Thanks to all my fellow oceanography friends in the department, it was great working with you and thanks to my loving room-mate, my sister, for always making me snacks whilst working on my project.

Contents

1 Introduction **1**

1.1 Objectives 3

2 Literature Review **5**

2.1 The Greater Agulhas Current System 5

2.2 Circulation of the Agulhas Current System 6

2.2.1 Source Regions of the Agulhas Current 7

2.2.2 Horizontal Structure of the Agulhas Current 8

2.2.3 Vertical Structure of the Agulhas Current 9

2.3 Volume transport of the Agulhas Current 11

2.4 Mesoscale, seasonal and interannual variability 13

2.5 Monitoring the Agulhas Current System 15

2.5.1 *In situ* Observations 15

2.5.2 Numerical Ocean Models 16

2.5.3 Satellite Observations and Altimetry 17

2.5.3.1 Monitoring volume transport using availiable oceanographic tools 18

3 Data and Methods **20**

3.1 The Hybrid Coordinate Ocean Model 20

3.2 The Agulhas Current Time-series Experiment 22

3.3 Development of the Agulhas transport proxy . . . 23
3.4 Recreating the Agulhas transport proxy in HYCOM . . . 25
3.4.1 Model Transport . . . 25
3.4.2 Model SSH . . . 25
3.4.3 Building the regression models . . . 26
3.5 Comparison of the transport proxy to actual model transports . . . 28
3.6 Sensitivity tests . . . 30

4 Results **32**
4.1 Proxy validation . . . 32
4.2 Evaluating the net transport proxy . . . 34
4.3 Sensitivity tests . . . 38
4.4 Investigating the transport variability . . . 39

5 Summary **44**
5.1 The Agulhas Current Transport Proxy . . . 44
5.1.1 Proxy Validation . . . 45
5.1.2 Evaluating the proxy performance . . . 46
5.2 Sensitivity tests . . . 47
5.3 Investigating the transport variability in HYCOM . . . 48

6 Conclusions and Future Research **52**
6.1 Conclusions . . . 52
6.2 Future Research . . . 54

Bibliography **55**

List of Figures

2.1 Source regions and structure of the Agulhas Current System. 9

2.2 Cross-track velocity structure of the Agulhas Current System 10

3.1 The HYCOM model configuration. 22

3.2 Geographical location of the ACT-mooring array. 24

3.3 Horizontal length scales of the SSH slopes. 26

3.4 HYCOM transport per unit distance proxies at the first model timestep. 29

4.1 Comparison of the transport time series obtained from the HYCOM proxy and the modelled HYCOM transport. 33

4.2 Annual correlation time-series between the HYCOM proxy and the modelled HYCOM transport. 34

4.3 Horizontal structure of the Agulhas Current during the highest and lowest correlated years. 35

4.4 Cross-track velocity structure of the Agulhas Current during the highest and lowest correlated years. 36

4.5 Cross-track velocity anomalies between the highest and lowest correlated years minus the development period. 37

4.6 Taylor diagram showing the results obtained from the sensitivity experiments on the net transport proxy. 39

4.7 Weekly time-series of the HYCOM proxy and modelled HYCOM transport during 2011. 40

4.8 Structure of the Agulhas Current during the weeks where there was a small difference between the proxy transport and the model transport. 41

4.9 SSH signal along the ACT array corresponding to individual transport events under evaluation. 42

4.10 Structure of the Agulhas Current during the weeks where there was a large difference between the proxy transport and the model transport. 43

A.1 HYCOM annual transport time series (T_{net}). 65

A.2 Taylor diagram showing the results obtained from the sensitivity experiments on the southwest transport proxy. 66

A.3 Linear regression models showing the relationship between HYCOM SSH slope and transport per unit distance for T_{net}. 67

A.4 Linear regression models showing the relationship between HYCOM SSH slope and transport per unit distance for T_{sw}. 68

List of Tables

2.1 Summary of volume transport estimates from previous observations in the Agulhas Current. 12

2.2 Summary of volume transport estimates from previous ocean modelling investigations. 12

2.3 Summary of transport proxy experiments using satellite altimetry. 19

3.1 HYCOM specifications. 21

3.2 Statistics for the 3-year HYCOM linear regression models. 27

3.3 Sensitivity experiment time periods. 30

4.1 Summary of the transport statistics of the HYCOM model transport against the HYCOM proxy transport. 33

4.2 Results obtained from calculating the net transport proxy over a range of time periods. 39

A.1 Results obtained from calculating the southwest transport proxy over a range of time periods. 66

Chapter 1

Introduction

The Agulhas Current System is the strongest western boundary current in the Southern Hemisphere and transports warm tropical water southward along the east coast of South Africa [Lutjeharms, 2006]. The Agulhas Current, in the northern region, is known for its narrow, fast, flow conditions following the steep continental slope [de Ruijter et al., 1999]. As the current continues southwestward the current separates from the continental shelf looping anticlockwise south of Africa, returning into the Indian Ocean as the eastward Agulhas Return Current [Beal et al., 2011; Biastoch and Krauss, 1999; Dijkstra and de Ruijter, 2001; Hermes et al., 2007; Lutjeharms, 2006; Loveday et al., 2014]. This is as a result of an increase in southward inertia, due to an accumulation of positive vorticity as the current progresses southwards [Dijkstra and de Ruijter, 2001; Loveday et al., 2014], and with the latitude of zero wind stress curl [Beal et al., 2011]. This region of retroflection, also referred to as the turbulent Cape Basin [Loveday et al., 2014], contains some of the highest levels of mesoscale variability measured in the global ocean [Gordon, 2003] and has a significant influence on the Atlantic Ocean, the Benguela upwelling system and the global overturning circulation system [Gordon et al., 1987; Beal et al., 2011; Durgadoo et al., 2013]. In the regional context, the Agulhas Current has a major influence on the local weather systems, due to the large latent and sensible heat flux, which contributes to rainfall and storm events over the adjacent land [Reason, 2001; Rouault et al., 2002; Rouault and Lutjeharms, 2003]. On the global scale, the Agulhas Current plays a significant role in the Atlantic Meridional Overturning Circulation (AMOC) as it stabilises the system by providing a salt-advective feedback through the process known as Agulhas leakage [Biastoch and Krauss, 1999; Beal et al., 2011; Durgadoo et al., 2013; Loveday et al., 2014]. The unique circulation of the Agulhas Current System, with

the interest in the regional and global climate, therefore makes it an important field of research.

In order to understand the dynamic nature and complicated flow regime of the Agulhas Current it is important to establish the strength and variability of the current. This can be done using numerical ocean models, satellite data and *in situ* observational data. Previous studies have suggested that measuring the dynamics of the Agulhas Current in the northern region is easier due to it's stable trajectory and it's confinement to the continental slope [van Sebille et al., 2010]. However, the close proximity of the current to the coast makes it difficult to monitor using satellite altimetry [Rouault et al., 2010]. In addition, the frequency of periodic disturbances in the event of a Natal Pulse and the interaction between the mesoscale eddies, originating from the source regions, with the western boundary current remain poorly resolved in many numerical ocean models [Tsugawa and Hasumi, 2010; Braby et al., 2016], thus highlighting the challenges involved in monitoring the dynamics in this region. Measuring the southern extent of the current, including Agulhas leakage, remains a difficult task due to higher levels of ocean turbulence [Gordon, 2003], which also makes this region difficult to simulate using numerical ocean models [Loveday et al., 2014].

There is evidently a trade-off between spatial and temporal sampling. *In situ* observations may accurately measure the dynamics of the Agulhas Current throughout the water column but are expensive and spatially coarse. Whereas, satellite observations can provide high-temporal, spatial data of the surface ocean but lacks detailed information below the surface. Together, satellite and *in situ* data should compliment one another. Additionally, numerical models are needed to provide coherent, high resolution data of the ocean throughout the water column, but are reliant on observations for boundary forcing conditions and validation purposes. Numerous studies aiming to monitor long-term changes in global current systems have adopted methods to combine the various sampling tools [eg. Andres et al. 2008; Imawaki et al. 2001; Maul et al. 1990; Yan and Sun 2015b; Zhu et al. 2004], including the recent development of the Agulhas transport proxy established to monitor the interannual variability and long-term trends in Agulhas Current transport [Beal and Elipot, 2016].

The Agulhas transport proxy was built based on the physical principle of geostrophy, where along-track sea surface height slope measured by the altimeter can be interpreted as a measure of the cross-track surface current. Previous studies have shown that a strong relationship exists between surface geostrophic velocity and full-depth transport [Elipot and Beal, 2015] and sea

level anomalies associated with the dynamics and variability of the Agulhas Current System make it particularly amendable to monitor using satellite altimetry [Fu et al., 2010; Rouault et al., 2010; Rouault and Penven, 2011] and therefore suitable to monitor using a satellite-transport proxy. The 22-year transport proxy created by Beal and Elipot [2016] assumed a fixed linear relationship between *in situ* transport and sea surface slope based on *in situ* measurements over a 3-year sampling period. Results from the Agulhas Current transport proxy experiment concluded that the Agulhas Current, as a western boundary current, has not intensified over the last two decades as was proposed by several climate models in their response to intensification of global wind systems and anthropogenic climate change [Cai, 2006; Yang et al., 2016], but has broadened as a result of increased eddy activity [Beal and Elipot, 2016].

1.1 Objectives

This study aims to recreate the Agulhas transport proxy, developed by Beal and Elipot [2016], within a regional HYCOM of the greater Agulhas Current System. Firstly, the relationship between model transport and model sea surface slope along ACT will be investigated. Following this, the impact of the vertical variability of the current, associated with current meanders or impacting mesoscale features, on the accuracy of the transport proxy will be assessed. Finally, the optimal length scale of observations needed to build a strong linear relationship between transport and SSH slope will be tested.

Will the strength of the linear relationship between transport and sea surface slope hold when extending the relationship over longer time-periods in HYCOM? Theoretically the vertical velocity structure changes during mesoscale meander events [Zhu et al., 2004] and thermohaline processes [Beal and Elipot, 2016] or even changes in the strength of the Agulhas Undercurrent may lead to changes in the vertical stratification. Will vertical variability in the model decrease the accuracy of the transport proxy. Finally, what would be the ideal sampling period needed to build a strong, linear relationship between transport and SSH slope. Building the linear relationship over periods, longer than 3 years, could perhaps increase the skill of the transport proxy, since the linear relationship would be independent and perhaps capture more current dynamics over the longer periods of time. This study motivates the need to improve long-term monitoring methods, where such improvements include advances in model development, combined with adequate validation studies, such as the current study, to help plan future experiments intending to monitor long-term changes in ocean circulation.

This thesis is structured as follows; Chapter 2 provides a detailed overview of the Agulhas Current System based on literature and previous experiments. Chapter 3 describes the data and methods, it should be noted that this section forms a key part of the thesis as the methods of recreating the proxy was a key aim of the study. Chapter 4 presents the results from the HYCOM transport proxy, Chapter 5 will discuss the results and relevant patterns aiming to address the objectives of the study and lastly Chapter 6 presents the final conclusions.

Chapter 2

Literature Review

2.1 The Greater Agulhas Current System

The Agulhas Current is the western boundary current of the South Indian Ocean flowing poleward along the east coast of Africa (∼27°S) to the south coast, offshore of the Agulhas Bank (∼40°S). The current is narrow, swift and strong and is suggested to be the strongest western boundary current in the global ocean based on volume transport in the core of the current [Lutjeharms, 2006]. The Agulhas Current system is key to the South African region due to its impact on the regional climate and has a large environmental and economic significance to the country, it also plays a significant role in the global ocean circulation [Beal et al., 2011].

The Agulhas Current's influence on the regional climate has a major impact on local weather systems including storm development and storm tracks, and the large moisture from the warm current contributes significantly to the frequency and strength of African precipitation [Rouault and Lutjeharms, 2003]. Several observational and modelling studies have investigated the variability of the Agulhas Current in association to changes in regional rainfall patterns [e.g. Walker and Mey, 1988; Jury et al., 1993; Lutjeharms and De Ruijter, 1996; Reason, 2001; Rouault and Lutjeharms, 2003] and have suggested that variability in heat transport or shifts from the mean position of the current is likely to have a direct influence on the local weather systems. Sustained long-term observations of the Agulhas Current, in addition to accurate weather forecasting, therefore provides valuable information to subsistence farmers [Rouault et al., 2000; Reason, 2001; Nakamura and Shimpo, 2004; Reason, 2002; Schouten et al., 2002; Palastanga et al., 2006; Gimeno et al., 2010] and fisheries along the east coast of South Africa, over the

Agulhas Bank [Roberts et al., 2010] and East African countries bordering the Greater Agulhas system. Lastly, the Agulhas Current is vitally important for the economic status of South Africa in terms of productivity and trade, ship routing, offshore industry and tourism.

The Greater Agulhas Current system plays a significant role in the ocean circulation system based on its location in the global ocean, it connects three of the major oceans; the Indian Ocean, the Atlantic Ocean and the Southern Ocean, each having unique circulation patterns and water mass characteristics. The Agulhas Current transports warm, salty, tropical water poleward, which in turn influences the oceanic heat flux and thus linkages between the ocean and atmosphere in the global context [Lutjeharms, 2006]. More specifically, the Agulhas Current advects large amounts of heat and salt into the Atlantic Ocean through a process known as the Agulhas leakage, which plays an important role in the Atlantic Meridional Overturning Circulation (AMOC) [Beal et al., 2011] contributing to the global mass balance [Ballegooyen et al., 1994]. Modelling studies have suggested that variability in Agulhas leakage can impact the strength of the AMOC by changing its stratification and its potential for deep convection [Weijer et al., 2001], which may have direct implications on the climate where strengthening (weakening) of the AMOC may lead to warmer (cooler) climate [Beal et al., 2011].

2.2 Circulation of the Agulhas Current System

Western boundary currents in the ocean are generated by the wind stress patterns over the subtropical basins and close off the anti-cyclonic basins in which they exist. Together, the easterly trade winds in the tropics and the westerlies at mid-latitudes apply a wind stress to the ocean gyre, thereby driving the general circulation regime, in particular western intensification. The wind stress applies a positive (negative) vorticity in the Southern (Northern) Hemisphere, resulting in equatorward Sverdrup transport. In order to balance the equatorwarrd transport and to conserve mass and potential vorticity the Sverdrup transport is balanced by a narrow, intense, poleward current thus allowing vorticity introduced by coastal friction to balance the vorticity input of the wind [Stewart, 2008]. The Agulhas Current System lies embedded in the South West Indian Ocean basin [Lutjeharms, 2006] and is primarily driven by the wind stress curl between the southeast trade winds and the southern hemisphere westerlies [Beal et al., 2011]. It is made up of a unique system of smaller flows from various source regions which contribute individually to the transport and variability of the main Agulhas Current. The source regions

are the eddies flowing through the Mozambique Channel, the East Madagascar Current and the recirculation of the Agulhas Return Current [Hermes et al., 2007; Stramma and Lutjeharms, 1997] (Figure 2.1).

When unravelling the dynamic nature of the Agulhas Current it is important to understand the dynamics of the source regions and hence the response of the Agulhas Current to associated disturbances and instabilities. Approaching instabilities may influence the mean current trajectory or change the vertical and horizontal structure of the current which, in turn, may influence the formation of baroclinic instabilities. Surface currents provide limited information on deeper currents and the exchange of water masses [Lutjeharms, 2006], which can be made clearer through hydrographic analyses, thus providing a clear understanding of the horizontal and vertical extent of the current, which can therefore provide additional information on the volume transport of the current and hence its role in the regional and global circulation regime.

2.2.1 Source Regions of the Agulhas Current

The South Equatorial Current (SEC) flows westward until it reaches the east coast of Africa where it splits flowing northward and southward into the Mozambique Channel. The circulation in the Mozambique Channel is dominated by southward moving eddies, mainly anticyclonic eddies [Ridderinkhof and De Ruijter, 2003; Halo et al., 2014] rather than a coherent current. These eddies propagate into the Agulhas Current [Schouten et al., 2002]. On the east coast of Madagascar the SEC bifurcates into the North (South) Eastern Madagascar Current (NEMC/SEMC) ultimately producing anticyclonic and cyclonic eddies (often dipoles) also moving into the Agulhas Current [Ridderinkhof and De Ruijter, 2003]. Past studies have shown that these eddies tend to destabilize the current trajectory on entrainment into the main current [Tsugawa and Hasumi, 2010], providing evidence of eddy dissipation in the northern Agulhas Current [Braby et al., 2016]. The third source is the recirculation of the Agulhas Return Current [Lutjeharms, 2006], which forms part of the Southwest Indian Ocean subgyre and recirculates back into the Agulhas Current at 65°E mainly south of Madagascar. Thus, to the best of our knowledge, the mean flow in the Agulhas Current is composed of approximately 25 Sv from the east of Madagascar and 35 Sv from recirculation, with only 5 Sv being contributed from the Mozambique Channel [Stramma and Lutjeharms, 1997; Hermes et al., 2007].

2.2.2 Horizontal Structure of the Agulhas Current

The Agulhas Current is split into a northern and southern region. The northern Agulhas Current forms at ~27°S and flows southward along the broadening continental shelf consequently growing in width up to ~33°S, where after it becomes the southern Agulhas Current [Lutjeharms, 2006]. Bryden et al. [2005] have shown that the variability in the northern current is small compared to the southern current. Except for the passage of Natal Pulses, causing the current to meander, the northern Agulhas Current can be found within 31 km of the coast 80% of the time [Gründlingh, 1980]. This stable current trajectory is due to the steep incline of the continental slope and its nearly linear downstream disposition [Lutjeharms, 2006] which therefore steers the current downstream close to the shelf edge. It is in the northern part of the current where the strongest flows are observed with average velocities of 1.5 m s^{-1}, occasionally exceeding 2 m s^{-1} [Krug and Tournadre, 2012; Rouault et al., 2010].

The southern Agulhas Current starts at ~33°S, where the continental shelf of the Agulhas Bank widens and separates from the coast [Lutjeharms, 2006]. As the current continues to move southward and offshore, the topographic steering force along the coast becomes smaller due to the increase in shelf width, this causes the current to meander forming cyclonic shear edge eddies, which increases the instability of the current. Thereafter, the current continues south-westward along the continental slope off the Agulhas Bank into the retroflection region [Lutjeharms, 2006].

The retroflection loop forms as the southern Agulhas Current leaves the Agulhas Bank and turns at the latitude of maximum westerly winds (~45°S) due to the strong southward inertia of the current, which overcomes the potential vorticity balance [Siedler et al., 2001]. The positive vorticity accumulation in the poleward-flowing jet results in a change of direction [Dijkstra and de Ruijter, 2001; Loveday et al., 2014] and thus causes the eastward flow of the Agulhas Return Current. The Agulhas Retroflection marks the end of the Agulhas Current and is the main source of Agulhas leakage [Beal et al., 2011]. Agulhas leakage being the process when salty, warm water is transported via large anti-cyclonic eddies, Agulhas Rings and filaments into the South Atlantic Ocean where it plays a vital role in the AMOC, forming an important component of the Earth's climate system, by transporting a substantial amount of heat from the warm Indian Ocean to the cooler Atlantic Ocean basin [Delworth et al., 2008].

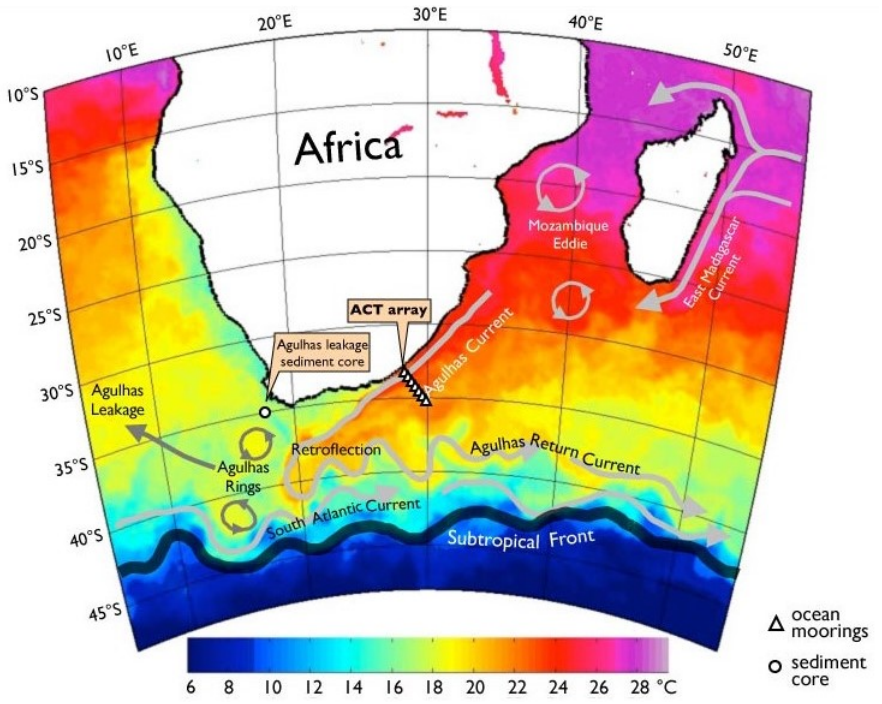

Figure 2.1: Source regions and structure of the Agulhas Current System. Source from http://act.rsmas.miami.edu/science/.

2.2.3 Vertical Structure of the Agulhas Current

The vertical structure of the Agulhas Current varies depending on its position relative to the continental shelf and therefore its latitude along the South African coast. Between Durban at 30°S and Port Edward situated 200 km downstream, the South African continental slope narrows and the maximum depth increases causing the Agulhas Current to become stronger [Schumann, 1981]. In order for the northern Agulhas Current to be stable at the shelf edge it must have vertical dimensions of sufficient extent [Lutjeharms, 2006] thereby ensuring that the vorticity structure of the current is appropriate in order to satisfy the condition of instability [de Ruijter et al., 1999]. It has been observed in the Agulhas Current that the position of strongest velocity at each depth moves offshore with increasing depth, thus revealing a v-shaped vertical structure, characteristic of western boundary currents [Beal and Bryden, 1999; Bryden et al., 2005; Beal et al., 2015]. Hydrographic sections have also revealed the density structure of the Agulhas to be typical of a western boundary current, with isopycnals sloping upward toward the coast thus marking strong poleward velocities (Figure 2.2). Furthermore, it has been shown that the Agulhas Current depicts an equivalent barotropic structure, meaning the current velocity does not change with depth, except for the presence of the Agulhas Undercurrent [Elipot and Beal,

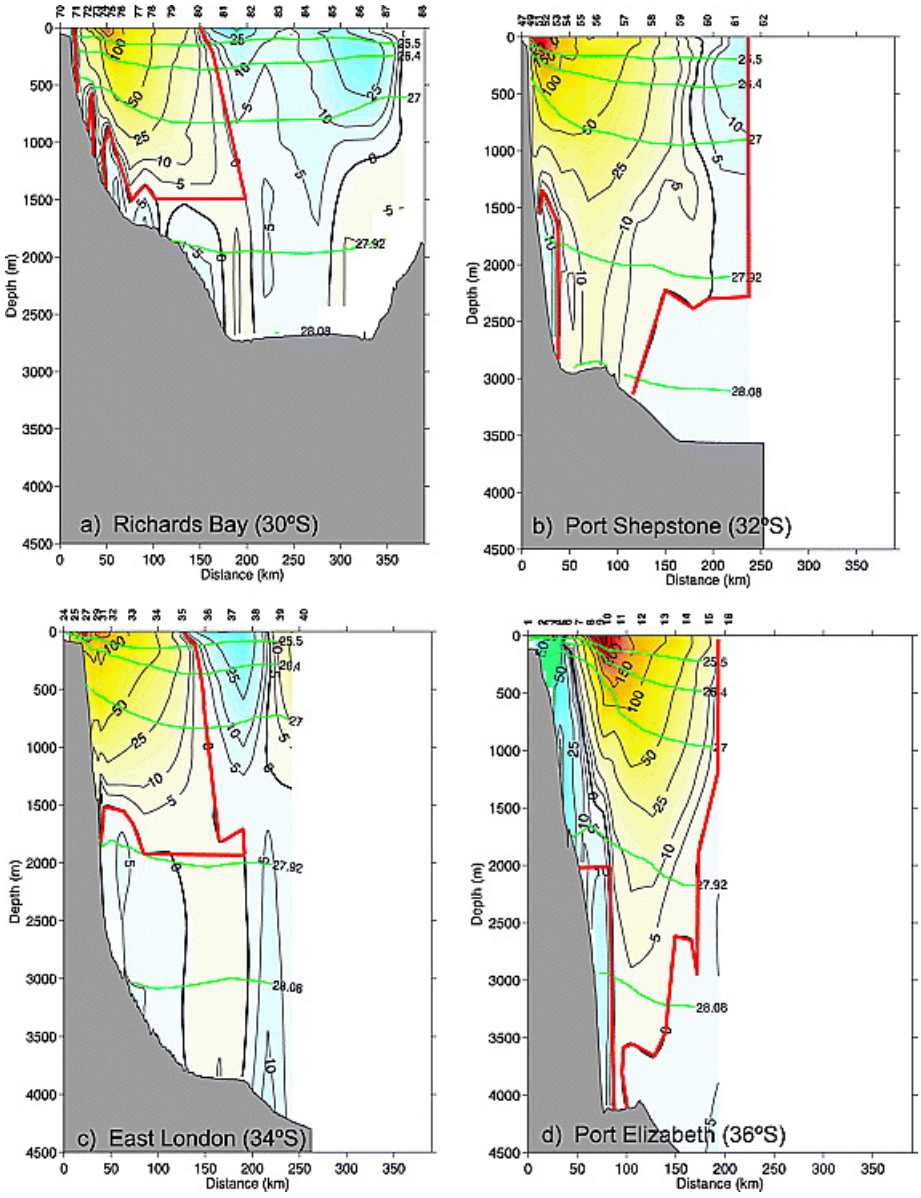

Figure 2.2: Model derived velocities showing the average vertical velocity structure of the Agulhas Current at a) 30°S Richards Bay b) 32°S Port Shepstone c) 34°S East London d) 36°S Port Elizabeth. Positive velocities (blue) indicate northward direction and negative velocities (yellow) indicate southward direction. The thick red lines delineate the Agulhas Current and the green lines represent the isopycnal density structure. Source from [Casal et al., 2009].

2015; Tsugawa and Hasumi, 2010]

A deep-water structural feature considered to be an essential component when working with vertical structure of the current is the Agulhas Undercurrent. Beal and Bryden [1999] presented observations of an undercurrent against the continental slope, at a depth of 1200 m. On average, the undercurrent appears as a sluggish northeastward flow, with an annual mean velocity of 10 cm s^{-1} [Beal and Bryden, 1999]. It "hugs" the continental slope between 1000 m depth and the

foot of the slope at 2900 m, between 11 km and 60 km offshore and appears to vary independently of the Agulhas Current particularly during meander events [Beal, 2009]. Bryden et al. [2005] found the vertical transition from the Agulhas Current to the undercurrent flow to be sudden, with no gradual rotation in current vectors and stated that this also provided an indication of strong topographic steering. Hence, it is essential to consider the undercurrent when calculating the volume transport of the Agulhas Current System.

2.3 Volume transport of the Agulhas Current

Many studies in the Agulhas Current System, aiming to monitor the strength and variability of the current have adapted various sampling methods, including observations, satellite data and numerical ocean models in order to successfully capture the current dynamics (Table 2.1 & 2.2). As part of the World Ocean Circulation Experiment (WOCE) in 1995, measurements of the transport and variability of western boundary currents at 30°S in each ocean were collected [Bryden et al., 2005]. Off South Africa, the Agulhas Current Experiment (ACE) took place between February and March 1995 and primarily focused on deploying an array of current meter moorings and full depth sections to make a synoptic transport measurement for a 267-day period at 32°S. [Gründlingh, 1983] showed that the variability in the position of the Agulhas Current was small in the Port Edward region therefore a current meter mooring array would work efficiently here. This experiment was expanded in Beal and Bryden [1997; 1999] where a full section volume transport of 71 Sv; 73 Sv ($1Sv=10^6 m^3 s^{-1}$) was calculated respectively. These were the first studies to include the undercurrent in its volume transport calculation.

More work was done on the ACE by Bryden et al. [2005] that measured the strength, variability, mean structure and transport of the Agulhas Current. The transport of the Agulhas Current was calculated using various methods: calculating the mean total transport and the poleward transport; summing only the negative velocities for the surface current as well as the mean undercurrent transport and the averaged equatorward transport by summing the positive velocities. This work highlighted the difficulties associated with volume transport estimates of the Agulhas Current as one should consider including contributions from nearshore or offshore eddies, separating the undercurrent from the volume transport equation and whether to use the mean transport or poleward transport.

The Agulhas Current Time-series experiment (ACT) was established to monitor the transport

Table 2.1: Summary of volume transport estimates from previous observations in the Agulhas Current.

Authors	**Location and Time**	**Transport**	**Method used / Reference level**
Gründlingh, 1980	32°S (ACE), 1975-1978	-20- -40 Sv	Geostrophic estimates
Gordon et al., 1987	32°S	-49 Sv	Current meters, 1500m
Toole and Warren, 1993	32°S, 1987	-85 Sv	Shipboard ADCP's, 2000m and wind stress data
Beal and Bryden, 1997	32°S, 1-year 1995-1996	-71 Sv	Current Meters: LADCP's and shipboard ADCP
Beal and Bryden, 1999	32°S, 1-year 1995-1996	-73 Sv	Mooring array current meters: LADCP's and shipboard ADCP
Bryden et al., 2005	32°S, 1-year 1995-1996	-70 Sv; -76 Sv	Mean total transport; Averaged poleward transport. Mooring array
Beal et al., 2015	34°S (ACT), 3-year 2010-2013	-77 Sv; -84 Sv	Net transport; Southwest transport; Mooring array: ADCP's, LADCP's and CPIES

*Negative values indicate transport in the southwest direction, 1 Sv= 10^6 m^3s^{-1}

Table 2.2: Summary of volume transport estimates from previous ocean modelling investigations.

Authors	**Location and Time**	**Transport**	**Ocean Model**
Lutjeharms and Webb, 1995	30°S; 36°S, 8-year model run	-90 Sv; -140 Sv	FRAM (Fine Resolution Antarctic Model), 1/2° x 1/4°
Biastoch and Krauss, 1999	30°S-35°S, 5-year climatological run	-47 - -67 Sv	MOM (Modular Ocean Model), 1/3°
Matano et al., 2002	32°S, 19-year (1979-1998) model run	-43 Sv	POCM (Parallel Ocean Circulation Model), 1/4°
Hermes et al., 2007	35°S, 12-year climatological run	-62 Sv	Climatological Mean from AGAPE, 1/3°
Backeberg et al., 2009	32°S, 11-year, 1996-2006	-58 Sv; -48 Sv	HYCOM O^4 (4^{th}order advection scheme); HYCOM O^2 (2^{nd}order advection scheme). 1/10°
Cooper, 2014	32°S, 8-year, 1993-2010	-70 Sv	HYCOM 1/12°
Loveday et al. 2014	32°S, 19-year climatological run	-70 Sv	ROMS: (ARC112) basin-scale nested 1/12° (1/4°)

*Negative values indicate transport in the southwest direction, 1 Sv= 10^6 m^3s^{-1}

and decadal variability of the Agulhas Current. The ACT array ran perpendicular to the south-east coast of South Africa, close to 34°S, downstream from the previous 1995 Agulhas Current

Experiment (ACE). They array was positioned below the TOPEX/Jason altimeter ground-track #96 and on the wide continental shelf, thus making it easier for mooring deployments [Beal et al., 2015]. The experiment consisted of two phases; a mooring array designed to capture the meandering state of the Agulhas Current [Beal et al., 2015] and the development of a twenty-year transport proxy to monitor the multi-decadal variability of the current [Beal and Elipot, 2016].

During the first phase of the experiment, from April 2010 to February 2013, the volume transport was calculated with two time series: The boundary layer transport (T_{box}) and the western boundary jet transport (T_{jet}) [Beal et al., 2015]. T_{box} is the net transport within a fixed distance of the coast and T_{jet} is the stream-dependent definition where boundaries of integration depend on the strength and cross-sectional area of the southwestward jet at each time step. The final boundary layer transport (T_{box}) amounted to -77±5 Sv and the western boundary jet transport (T_{jet}) to -84±11 Sv [Beal et al., 2015], the negative sign indicating transport in the southwest direction. Beal et al. [2015] concluded that the increase in transport in comparison to the ACE volume transport may be due to the increase in Sverdrup transport over an increase in latitude. Recently, the ACT experiment has been re-established by the ASCA array (Agulhas System Climate Array) to continue monitoring the current and its impact on the regional and global climate, including measurements of heat and salt exchange across the passage of the array [Morris et al., 2017 (in press)]. Agulhas Current transport variability directly induces variability in the heat exchange which further impacts current processes downstream, such as Agulhas leakage and the AMOC [Lee et al., 2011], thereby encouraging increased monitoring effort in the current. The ACT experiment is of particular importance to the current investigation and is discussed in more details in the methods section.

2.4 Mesoscale, seasonal and interannual variability

The most dominant mode of variability in the northern Agulhas Current originates from instabilities that develop in the region north of Durban, known as the Natal Bight [de Ruijter et al., 1999; Bryden et al., 2005; Lutjeharms, 2006]. These instabilities, commonly known as Natal Pulses, cause the current core to shift offshore which generally results in a weakened current velocity followed by an apparent surfacing of the Agulhas Undercurrent with a northward flow over the continental slope [Bryden et al., 2005]. Three to five pulses are observed each year and propagate southwestward along the coastline [Lutjeharms et al., 2001]. Rouault and Penven

[2011] observed an average of 1.6 meander events per year which was corroborated by Elipot and Beal [2015]. Bryden et al. [2005] suggested that the overall volume transport weakens during meander events but further work by Leber and Beal [2014] showed that there is no significant change in the Agulhas Current transport during a meander, because weakening of the current core is accompanied by a broadening of the core to conserve the transport.

The seasonality of the Agulhas Current transport remains a matter of debate based on various contradicting results, where ocean models have predicted a seasonal cycle with weaker transports in austral summer-fall (February-April) and strongest in winter-spring (August-October), suggesting that the tropical winds influence the flow of the Agulhas Current via the Mozambique Channel [Matano et al., 2002]. However, other estimates based on along-track satellite altimetry data have shown maximum surface geostrophic currents in the austral-summer [Krug and Tournadre, 2012]. Whereas, *in situ* studies showed a maximum transport in summer (March) and minimum in winter (August) [Beal et al., 2015; Beal and Elipot, 2016], displaying a similar cycle to the Gulf Stream and the Kuroshio [Sato and Rossby, 1995]. This cycle is however not successfully captured by model simulations [Vermeulen et al., (in prep)] and does not match the cycle predicted by Sverdrup transport [Hutchinson, pers comm].

Due to the lack of *in situ* observations and limitations of numerical models, less is known about the inter-annual to decadal variability of the Agulhas Current. However, it has been suggested that mesoscale anomalies such as meander events and Agulhas Rings have inter-annual variability linked to the Indian Ocean Dipole and El Nino Southern Oscillation modes [Beal et al., 2015]. Other studies have suggested that there is a spin up of the subtropical gyres in the Southern Hemisphere in response to the intensification of wind stress curl over mid-latitude regions associated with the SAM (Southern Annular Mode) over the same period [Beal and Elipot, 2016; Cai, 2006; Saenko et al., 2005]. This may lead to an intensification and a poleward shift of the western boundary currents [Yang et al., 2016] which would occur over decadal to centennial time scales. Another study by Durgadoo et al. [2013] concluded that Agulhas leakage predominantly responds to inter-annual changes in westerly wind stress and showed that the poleward displacement of the westerly wind belt reduces Agulhas leakage. Therefore, addressing the question of inter-annual and decadal variability requires fundamental knowledge of associated oceanic and atmospheric dynamics, thus making it intricate, but interesting research.

2.5 Monitoring the Agulhas Current System

2.5.1 *In situ* Observations

The ocean state is routinely monitored by various sensors from platforms such as ships, moorings, drifters and relatively new platforms such as the autonomous Argo floats and gliders [Schiller and Brassington, 2011]. The provision of *in situ* data has therefore significantly increased over the past decade since it can provide valuable information about the ocean state. However, monitoring the ocean using *in situ* methods is often expensive and spatially restricted.

The Agulhas Current has been monitored for many years using *in situ* methods. Several studies aiming to resolve the dynamics of the current and its source regions include mooring and ship-based transect routes across different regions in the current. The ACE mooring array measured the volume transport across the Agulhas Current at 32°S from February to Novemeber 1995 [Bryden et al., 2005] and further downstream, ∼34°S, ACT and currently the ASCA array monitor the Agulhas Current transport and variability [Beal et al., 2015; Beal and Elipot, 2016; Morris et al., 2017 (in press)]. Studies focussing on the southern Agulhas region include the Crossroads transect route that is annually sampled via the *RV Agulhas II* to measure the dynamics of the current as it moves over the Agulhas Bank as well as a portion of the Agulhas Return Current and the exchange of water masses between the Indian and Atlantic Ocean [Ansorge et al., 2013]. Lastly two key experiments that focus on the dynamics of the Agulhas Retroflection and Agulhas Rings include the SAMBA (South Atlantic Moored Buoy Array) as part of the SAMOC (South Atlantic Merdional Overturing Circulation) initiative which builds onto the key results obtained from another important observing line- the Goodhope transect [Ansorge et al., 2014]. SAMBA forms part of a collaborative initiative between South African, French, Brazilian and US oceanographers, and together with an observational array along the northern section of the Goodhope transect they aim to monitor changes in the AMOC and hence the influence of the Agulhas Leakage on the climate [Morris et al., 2017 (in press)].

Though Argo floats, drifters, gliders and satellite measurements continue to revolutionise the study of the upper ocean, there is still a need to study the full ocean depth with moored instruments [Ansorge et al., 2014]. Full-depth current meter moorings can measure current speeds of the entire water column up to 4000 m deep and for hundreds of kilometers across the ocean, but in order to calibrate the instruments on the mooring-array or sensors on the autonomous profiling

platforms additional hydrographic data needs to be collected on ship-based transects via CTD casts, XBTs and underway sampling. Therefore obtaining *in situ* data remains a difficult task but is necessary to improve our understanding of the dynamics of the Agulhas Current System or any other region in the global ocean.

2.5.2 Numerical Ocean Models

Modelling the Agulhas Current System over the past decade has become a top research priority in the oceanographic discipline due to the significant role the Agulhas Current plays in the global circulation and hence the global climate and the sparse observations available to quantify this relationship. The Agulhas Current has been successfully simulated, from its sources to the spawning of the Agulhas Rings, using regional and global ocean models [Penven et al., 2011]. However, the incredibly dynamic nature of the current, along with the lack of long-term observations have made the validation of realistic numerical models in this region very challenging.

The first realistic simulation of the Agulhas Current in the Fine Resolution Antarctic Model (FRAM) [Lutjeharms and Webb, 1995] clearly simulated the Agulhas Retroflection and Agulhas Rings. However, certain biases involved in the Agulhas Retroflection dynamics in the FRAM simulation, such as the early retroflection and the inaccurate trajectory of the Agulhas Rings into the South Atlantic, were also observed later in other ocean models. Over time this bias has been reduced (or even removed) by improving numerical precision, incorporating better model physics [Backeberg et al., 2009], or by improving the conservation properties of the momentum advection scheme [Bernard et al., 2006]. With the advancement in numerical model configuration and observational data programmes, global forecast/reanalysis products have improved in spatial resolution therefore making them more applicable over regional domains, such as in the Agulhas Current, where the flow regime is now better understood than in the past. However, small biases remnant in various numerical models emphasize the need to continue to investigate the Greater Agulhas Current System [Penven et al., 2011]. Thus, using the global modelling systems along with independent observational data sets and available literature we are able to create a robust and consistent method to evaluate future regional models of the Agulhas Current System.

2.5.3 Satellite Observations and Altimetry

Satellite altimetry in oceanography has developed rapidly in the 21st century and with the increasing techniques and capabilities it is still emerging. Recognising homogenous, geostrophic flow in the Agulhas Current (Equations 2.1) and assuming hydrostatic balance (Equation 2.2) satellite altimetry, through the use of the geostrophic approximation (Equations 2.3), has enabled scientists to estimate the transport in the upper layers of ocean currents all around the world [Siedler et al., 2006]. The broad temporal and spatial data from satellites has also made it easier to monitor the dynamics of the Agulhas Current System, providing a cost-effective alternative to *in situ* measurements and the datasets provide vital inputs to ocean modelling systems for data assimilation schemes and validation purposes. The geostrophic approximation measures surface current velocities using the equations below:

$$u = -\frac{1}{f\rho}\frac{\partial p}{\partial y} \qquad v = \frac{1}{f\rho}\frac{\partial p}{\partial x} \tag{2.1}$$

$$\frac{\partial p}{\partial z} + \rho g = 0 \tag{2.2}$$

$$fu = -g\frac{\partial \eta}{\partial x} \qquad fv = g\frac{\partial \eta}{\partial y} \tag{2.3}$$

where f is the Coriolis force dependent on latitude, u and v are the zonal and meridional geostrophic velocities, g is the gravitational acceleration,ρ is the ocean density, p represents the pressure and and η represents the sea surface height. Altimetry is a valuable tool that has often been used to track changes in the Agulhas Current in the past Krug and Tournadre [2012]. However, the narrow proximity of the current to the coast, particularly in the northern region, does limit the usage of merged altimetry products, due to coastal contamination, atmospheric errors or inaccurate mean dynamic topography (MDT) estimates from complimentary data sources [Rouault et al., 2010]. An alternative technique to compliment altimetry in coastal regions was through the usage of ASAR (advanced synthetic aperture radar) observations [Rouault et al., 2010]. Similary, SAR imagery could provide means of mapping ocean currents from the open ocean to the coast at a high resolution, using the Doppler shift method, which simply allowed one to derive estimates of the surface current velocity in the line of sight of the radar [Chapron et al., 2005]. Other applications of altimetry such as investigating volume transport in the Agulhas Current [Beal and Elipot, 2016], seeks to recover information about the sub-surface structure

of the ocean and not all ocean processes causing variations in sea surface height are associated with full-depth dynamics and therefore do not have clear surface signatures. Therefore, unless an ocean current depicts a barotropic structure, simple assumptions about the vertical structure of the current would allow altimetry to "see" below the surface [Robinson, 2004]. Another method would be to model the depth variability and then use the satellite data to validate the predictions of the sea surface. Altimetry is therefore a powerful observing tool, however combining it with new, modern observing techniques and using the data in robust algorithms could further increase its value.

2.5.3.1 Monitoring volume transport using availiable oceanographic tools

Due to spatial and temporal limitations of *in situ* data and unresolved processes in models, scientists rely on multi-decadal altimetry data to measure long-term ocean circulation patterns. This however does not make hydrographic or model data less essential, as a comprehensive set of *in situ* and satellite data is needed to enable ocean product algorithms to be developed [[Robinson, 2004]], and allow ocean models to validate the observations and hence the algorithms. Various studies have recently utilised satellite altimetry measurements as a proxy for monitoring transports of ocean currents around the globe, of which some aimed to monitor a long-term transport record of the Kuroshio Current [Imawaki et al., 2001; Zhu et al., 2004; Andres et al., 2008; Yan and Sun, 2015a] the Gulf stream [Maul et al., 1990] and another of the Agulhas Current [Beal and Elipot, 2016].

Based on the results from the proxy experiments in Table 2.3, it was predicted that a similar relationship between transport and satellite altimeter data may hold for most western boundary currents [Imawaki et al., 2001]. In each experiment the transport proxy is based on three assumptions, (1) oceanic flows tend to be in geostrophic balance with surface velocities proportional to surface slope (2) ignoring effects due to vertical changes in the current structure, hence an equivalent barotropic structure and (3) a fixed regression relationship between transport and sea surface slope.

The current study aims to test these assumptions by investigating the relationship between volume transport of the Agulhas Current and the gradient of sea surface height, across the ACT array, using a regional Hybrid Coordinate Ocean Model. This work will complement previous studies to further understand the need for coherent, *in situ* and satellite based observing systems in support of ocean and climate research.

Table 2.3: Summary of transport proxy experiments using satellite altimetry.

Author	**Location**	**Method**
Maul et al., 1990	Gulf Stream, Straits of Florida	Correlation between Pegasus volume transport estimates from 1982-1984 and sea level measurements from cable and weather data (1992-1988) to create a 6-year transport time series.
Imawaki et al., 2001	ASUKU array across the Kuroshio, South of Japan	Correlated *in situ* transport measurements (1993-1995) to SSH difference from the (TOPEX/POSEIDON) altimeter across array to estimate 7-year transport time series (1992-1999).
Zhu et al., 2004	Ryukyu current across the O-line, Southeast of Okinawa Island, Japan	Correlated ocean mooring data (2000-2001) to T/P SSH and tide gauge data to obtain 9-year (1992-2001) transport time series.
Andres et al., 2008	Kuroshio transport across the C-line in the East China sea, 28°N	Apply empirical relationship between 13-month (2003-2004) *in situ* observations and SLA difference (T/P, Jason1) across 210km array to obtain 12-year transport measurement (1992-2004).
Yan and Sun, 2015a	Kuroshio inflow northeast of Taiwan Island, WOCE PCM-1 mooring array	Correlation iteration scheme to find optimal index for Kuroshio inflow. East Taiwan Channel (ETC) mooring data (1994-1996) is highly correlated with ADT SSH variation across P1-P2 from the merged satellite product. Use 10-year HYCOM output to validate proxy time-series.
Beal and Elipot, 2016	ACT array across the Agulhas Current (34°S), South Africa	Build nine linear regression models between sea surface slope (T/P, Jason-1 & 2) and transport per unit distance calculated from *in situ* data (2010-2013) for each mooring site. 22-year transport proxies (*Tbox* & *Tjet)* from 1993-2015.

*** Assumptions:** Geostrophy, equivalent barotropic current structure and a fixed regression relationship.

Chapter 3

Data and Methods

3.1 The Hybrid Coordinate Ocean Model

The Hybrid Coordinate Ocean Model (HYCOM) is a primitive equation ocean model that was developed from the Miami Isopycnic Coordinate Ocean Model (MICOM) [Smith et al., 1990]. HYCOM combines optimal features of isopycnic-coordinate and fixed-grid ocean circulation models into one framework [Bleck, 2002] and uses the hybrid layers to change the vertical coordinates depending on the stratification of the water column. The model makes a dynamically smooth transition between the coordinate types via the continuity equation using the hybrid coordinate generator [Chassignet et al., 2007]. Well-mixed surface layers use z-level coordinates, ρ-coordinates are utilized between the surface and bottom layers in a well-stratified ocean, and the bottom layers apply σ-coordinates following bottom topography. Adjusting the vertical spacing between the hybrid coordinate layers in HYCOM simplifies the numerical implementation of several physical processes without affecting the efficient vertical resolution, and in doing so combines the advantages of the different coordinate types in optimally simulating coastal and open-ocean circulation features [Chassignet et al., 2007].

The HYCOM output in the current investigation comes from a nested configuration where a basin-scale model of the Indian and Southern Ocean (INDIA) [George et al., 2010] provides boundary conditions to a 1/10° model of the Agulhas Current (AGULHAS) [Backeberg et al., 2008; 2009; 2014]. The regional nested model, AGULHAS, received boundary conditions from the basin-scale model [George et al., 2010] every 6-hrs with snapshot fields. The boundary conditions were relaxed towards the outer model over a 20 grid cell buffer zone. The horizontal resolution

Table 3.1: HYCOM specifications.

Model	HYCOM (regional)
Configuration	AGULHAS (nested)
Nested domain	0°-60°E; 10°-50°S
Time period	1980-2014
Resolution	1/10°
Grid spacing (km)	~10km
Vertical discretization	30 hybrid layers
Bathymetry	GEBCO 1'
Atmospheric forcing	ERA-interim reanalysis data (1/4°) resolution
Boundary forcing	Parent model (INDIA)
Advection scheme	2^{nd} order
Vertical mixing scheme	KPP

of the parent model ranged from 14 km in the northern Indian Ocean to 45 km in the Southern Ocean, with a resolution ranging from 30-40 km in the region of the Agulhas Current. The nested model covered the region from the Mozambique Channel up to the Agulhas Retroflection region and the Agulhas Return Current, geographically extending from approximately 0°-60° East and from 10°-50° South, with a horizontal resolution of ~10 km that adequately resolved mesoscale dynamics to the order of the first baroclinic Rossby radius estimated to be about 30 km [Chelton et al., 1998] (Figure 3.1). Both models have 30 hybrid layers and targeted densities ranging from 23.6 to 27.6 kg/m^3.

The parent model was initialised from Levitus climatology (WOA05) [Antonov et al., 2006] and spun up for 10 years using climatological ERA-interim forcing [Dee et al., 2011]. AGULHAS was initialised from a balanced field of the parent model interpolated to the high-resolution grid. Both models were then run from 1980 to 2014 using interannual forcing from ERA40 [Uppala et al., 2005] and ERA-interim [Dee et al., 2011]. Version 2.2 of the HYCOM source code has been used in this model and together with the second order advection scheme that provides an

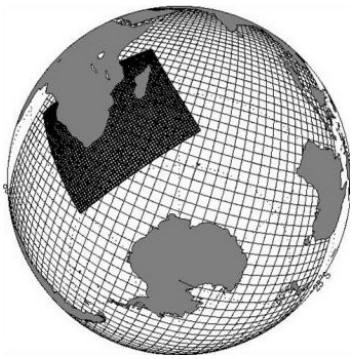

Figure 3.1: The HYCOM model configuration. Coarse resolution, basin-scale model grid (INDIA) provides boundary conditions for a high resolution nested model grid (AGULHAS). Every 10^{th} grid cell produces the mesh grid. Source from Backeberg et al. 2008.

improved representation of the Agulhas Current [Backeberg et al., 2009]. However, limitations of the free running model include high levels of SSH variability south of Madagascar and offshore of the Agulhas Current, suggesting that eddy trajectories in the model are too regular and consistent [Backeberg et al.,2009; 2014]. The data available for this study was a weekly output of the regional HYCOM model of the Agulhas region from 1980 to 2014. See table 3.1 for a summary of the model configuration.

3.2 The Agulhas Current Time-series Experiment

The Agulhas Current Time-series Experiment was established to obtain a multi-decadal proxy of Agulhas Current transport using satellite altimeter data. The first phase of the experiment was the *in situ* phase where the ACT mooring array was deployed in the current for a period of three years [Beal et al., 2015]. The second phase was the development of the transport proxy, where sea surface height along the ACT section, obtained from satellite altimetry, was regressed to the *in situ* transport measurements [van Sebille et al., 2010; Beal and Elipot, 2016]. To optimally facilitate the regression between the transport and altimetry, the ACT array was collocated with the altimeter track number 96 successively occupied by satellites TOPEX/Poseidon (1992-2002), Jason-1 (2002-2008) and currently Jason-2 (since 2008) and Jason-3 (since 2016) [Beal and Elipot, 2016] (Figure 3.2a).

During the first phase of the ACT experiment, the mooring array was maintained in the Agulhas Current for a period of 34 months, from April 2010 to February 2013, perpendicular to the continental slope at 34°S, south of East London, South Africa (Figure 3.2). The array was made up of 12 stations; stations A through G were full-depth current meter moorings which

were, on average, 26km apart. Station P1 was a coastal tide gauge and stations P2-P5 were CPIES (Current- and Pressure-recording Inverted Echo Sounders) placed 50km apart (Figure 3.2b). The CPIES were used to estimate the geostrophic cross-track velocity beyond the end of the mooring array so that the Agulhas Current variability was fully-captured during meander events [Beal et al., 2015]. During the ACT experiment the volume transport was calculated with two time series: The boundary layer transport (T_{box}) and the western boundary jet transport (T_{jet}). T_{box} is the net transport within a fixed distance of the coast while T_{jet} is the stream dependent definition where boundaries of integration depend on the strength and cross-sectional area of the southwestward jet at each time step. The western boundary jet transport algorithm was developed to specifically exclude the bias in transport during meander events, particularly during the occurrence of an inshore counter flow [Beal et al., 2015].

During the second phase of the experiment, Beal and Elipot [2016] built a 22-year proxy by regressing the three years of *in situ* measurements, obtained from the first phase of the experiment, to satellite altimeter data spanning the years 1993-2015. Development of satellite altimetry over the years has improved methods to monitor ocean circulation considering the spatial and temporal limitations involved with *in situ* monitoring [Yang et al., 2001]. However, when inferring a trend in a current structure based on satellite altimetry it is important to understand the relationship between sea surface height and transport and to be cautious regarding the assumptions used to validate the proxy [Beal and Elipot, 2016]. In order to obtain transport estimates using altimetry, it was also important to define accurate current boundaries, therefore the T_{box} proxy was developed to estimate transport trends of the fixed Agulhas Current and the T_{jet} proxy to capture the transport variability of the meandering jet.

3.3 Development of the Agulhas transport proxy

Based on the physical principle of geostrophy, sea surface slope is proportional to surface geostrophic velocity. Previous analyses have shown the structure of the Agulhas Current to be equivalent barotropic [Elipot and Beal, 2015], meaning the current velocity direction does not change with depth [Tsugawa and Hasumi, 2010; Lin and Che, 2012]. This suggests that the relationship between surface geostrophic velocity and full depth transport should be strong, despite the presence of the Agulhas Undercurrent [Beal and Elipot, 2016]. The relationship between sea surface slope and transport was therefore tested using linear regression models, which explicitly described a relationship between the predictor variable, sea surface slope and the response

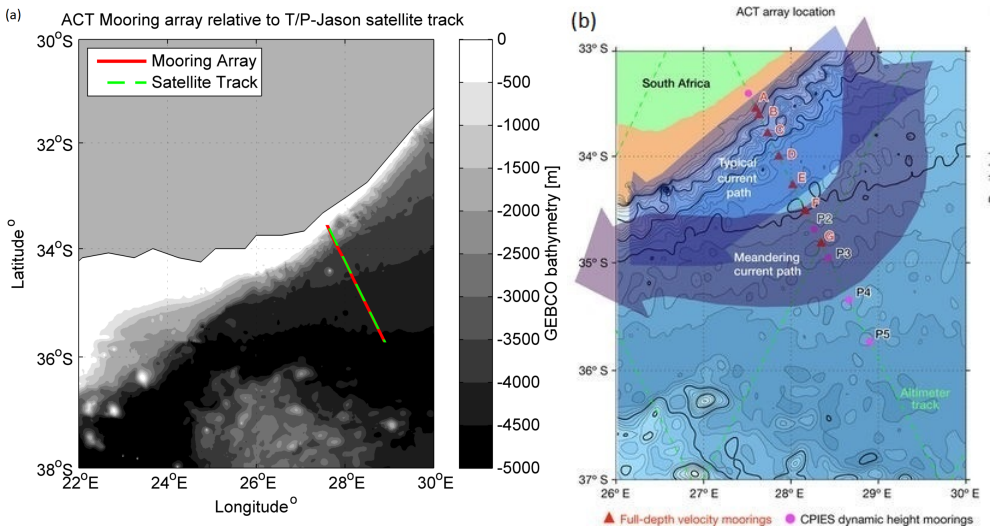

Figure 3.2: (a) Geographical location of the ACT-mooring array (red) relative to the T/P, Jason-1,2,3 satellite track #96 (green-dashed). Grey shading illustrates the GEBCO bathymetry (m). (b) Instrumentation along the ACT array, consisting of current meter moorings A-G and CPIES (Current Pressure Inverted Echo Sounders) sites P2-P5 (Source from Beal and Elipot, 2016).

variable, transport per unit distance [van Sebille et al., 2010; Beal and Elipot, 2016].

The transport proxy created by Beal and Elipot [2016] was initially developed by finding a linear relationship between transport and sea surface slope across the length of the ACT array, a common method used in previous studies [Imawaki et al., 2001; van Sebille et al., 2010; Sprintall and Revelard, 2014; Yan and Sun, 2015a]. However, this method lead to uncertainty in the linear regression relationship due to the strong, co-varying sea surface height across the current. The preferred method was therefore to build nine individual linear regression models, one for each mooring position and CPIES-pairs along the ACT array, which linearly related local transport to the local sea surface slope [Beal and Elipot, 2016]. It is important to note that the regression proxy assumed a constant, linear relationship over the three-year *in situ* period and the transport variable in the regression models essentially referred to transport per unit distance (Tx and $Txsw$), the vertically integrated velocity measured in $\mathrm{m^2 s^{-1}}$. The total transports, T_{box} and T_{jet} measured in $\mathrm{m^3 s^{-1}}$, were calculated by integrating the Tx and $Txsw$ estimates, predicted from the regression models, to the respective current boundaries. In the current study the boundary layer transport (T_{box}) will be referred to as the net transport (T_{net}) and the western boundary jet transport (T_{jet}) will be referred to as the southwest transport component (T_{sw}). The transport per unit distance will remain Tx and $Txsw$ for the net and southwest transport regression models.

3.4 Recreating the Agulhas transport proxy in HYCOM

3.4.1 Model Transport

In order to recreate the Agulhas Current proxy in HYCOM, a virtual version of the mooring array was developed in the model. The mooring velocity field in the model was created by extracting the barotropic velocity from each mooring location (A-G) and CPIES-pair P3-P4, P4-P5 for the 34-year model period. Extracting the barotropic velocity component from each mooring avoided interpolation errors that may have occurred if the model velocity was interpolated onto the locations of each current-meter instrument on each mooring [eg. van Sebille et al., 2010]. To build the regression models the transport per unit distance and sea surface slope for each of the nine mooring locations were calculated (hereafter CPIES-pair P3-P4 and P4-P5 were included as mooring positions 8 and 9). Transport per unit distance (Tx) for each mooring was calculated by integrating the cross-track barotropic velocity with the respective depth at each mooring location. The same method was employed to build the regression models for the southwest transport by excluding the northeast cross-track barotropic velocity components from the gridded velocity field hence only including the southwestward flow ($Txsw$).

In line with the objectives of the study, the HYCOM transport proxy was compared to the simulated transport extracted from HYCOM in order to investigate the differences between the proxy and actual modelled transport and hence understand which processes the proxy failed to represent. The transport across the ACT section was extracted by setting up the grid points between the two coordinates defining the start and end of the section following the great circles of the sphere and calculating the defined transport at each grid point along the section. The transport calculation facilitated a separation of the transports into two components: the net transport component (T_{net}) and the southwest transport component (T_{sw}).

3.4.2 Model SSH

In order to reproduce the "along-track" SSH altimeter data to create the proxy, 34 years of HYCOM SSH was linearly interpolated onto the coordinates of the TOPEX/Jason satellite track 96 overlapping the model ACT array. The coordinates were obtained from the filtered 12 km Jason-2 Aviso satellite product, and not the unfiltered 6 km product as was used for the original ACT proxy [Beal and Elipot, 2016], since the 12 km product matched the ∼10 km model

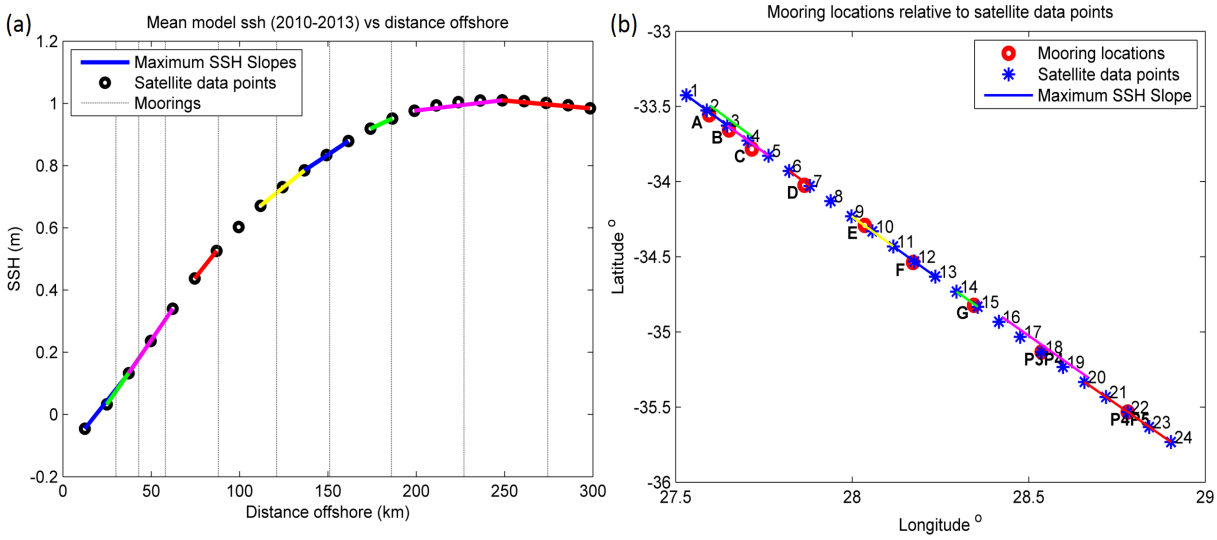

Figure 3.3: Optimal SSH data points chosen to maximise the correlation between $Tx/Txsw$ and SSH slope. a) Maximum slopes between moorings relative to the offshore SSH slope during 2010-2013 b) Length scales of the SSH slopes between the satellite points relative to the positions of the moorings.

resolution more closely. To obtain the sea surface slope for each regression model, an optimal pair of SSH data points was chosen such that the horizontal length scale between them allowed for a maximum correlation between the sea surface slope and Tx. The individual SSH slopes therefore account for the covarying sea level along the length of the array [Beal and Elipot, 2016]. The length scales of the slope ranged from 24 km at mooring A to 12 km at mooring G and 48 km for the offshore CPIES-pairs, indicating an increase in the spatial scale of offshore flow, possibly due to offshore variability (Figure 3.3). Results from the *in situ* proxy experiment by Beal and Elipot [2016] also showed an increasing length scale with increasing distance offshore, however the results varied considerably in magnitude given the length scale of 27 km at mooring B to 102 km at mooring G.

3.4.3 Building the regression models

Nine linear regression models were developed to estimate the transport per unit distance *(Tx* and *Txsw)* from the HYCOM sea surface slope during the same three-year period over which the ACT proxy was developed (2010-2013). Calculating the model transport proxy over the same three years as the *in situ* ACT proxy was simply to validate the methods in the model. Further tests were later performed, where the proxy was calculated over a range of different time periods (refer to section 3.6).

The coefficient of determination (R^2) from the regression models showed how well the linear

relationship predicted the transport per unit distance estimates from HYCOM (Table 3.2). The R^2 statistics from the regression models (Appendix) ranged from 0.86 at mooring A (30 km offshore) to 0.49 at the last CPIES-pair P4P5 (275 km offshore) for the net transport proxy and 0.86 at mooring A to 0.37 at P4P5 for the southwest transport proxy (P values $< 10^{-3}$). Results from the *in situ* proxy experiment showed an increase in the R^2 statistics ranging from 0.51 at mooring A and 0.81 for CPIES-pair P4P5 for the net transport proxy [Beal and Elipot, 2016], thus suggesting that the regression models had poorer skill inshore during the *in situ* experiment, whereas HYCOM showed an opposite trend. The results from the southwest transport regression models in HYCOM showed similar results for the inshore mooring locations (A, B, C, D, E) with slightly higher correlations for offshore moorings F, G and CPIES-pair P3P4 but a lower correlation for D and the furthest CPIES-pair P4P5. This suggests that the *Txsw* regression models explained more variance for moorings F, G and P3P4 but less variance for D and P4P5 than the *Tx* regression models. The regression coefficients, representing the rate of change of transport as a function of SSH slope, suggests that at mooring A, 1 cm increase in SSH per km increases *Tx* by 278 m^2s^{-1}, similarly for the *Txsw* and 1 cm increase in SSH per km for CPIE-pair P4P5 increases *Tx* and *Txsw* by 1233 m^2s^{-1} and 656 m^2s^{-1} respectively (Appendix, Figures A3 & A4).

Table 3.2: R^2 statistics for the 3-year HYCOM linear regression models.

Moorings	**R^2**	
	Tx	*Txsw*
A	0.86	0.86
B	0.75	0.75
C	0.75	0.75
D	**0.49**	**0.48**
E	0.62	0.62
F	**0.60**	**0.72**
G	**0.55**	**0.65**
P3-P4	**0.46**	**0.49**
P4-P5	**0.49**	**0.37**

*P-values < 0.05 (all significant at a 95% confidence interval)

To calculate the total transport across the ACT array requires continuous *Tx* estimates across the current. This was achieved by fitting a piecewise cubic Hermite interpolating polynomial function (Matlab®: pchip) to obtain transport estimates at 1 km intervals from the coast to the

end of the array. Fitting the transport function to the coast and equating it to zero would be equivalent to fitting a non-slip boundary condition in the model (Figure 3.4). Before calculating the total transport the current boundaries were defined. The net transport (T_{net}) was calculated by integrating Tx horizontally to 230 km offshore, the 3-year mean width of the current in HYCOM. The southwest transport (T_{sw}) was calculated using the algorithm developed in Beal et al., 2015 by integrating *Txsw,* the southwest transport component, to the first maximum of Tx beyond the half-width of the current (115 km) at each time step (Figure 3.4). T_{sw} therefore encompassed the meandering structure of the Agulhas Current.

In order to test the accuracy of the transport proxy, it was compared to the HYCOM transport for the same period over which the proxy was developed (2010-2013) to identify differences, and by studying the corresponding model fields, identifying features the proxy failed to represent. The correlation for the overlapping transports from the model and the model proxy was calculated as well as the 3-year mean and standard deviation. Assuming the constant three-year linear relationship derived over the period, 2010-2013, the linear relationship was extended to the entire 34-year model time period. This resulted in transport per unit distance estimates (Tx and *Txsw)* for each mooring position from 1980 to 2014. Thereafter the 34-year transport proxy was calculated by applying the same methods that were used to calculate the 3- year time-series; firstly, obtaining Tx estimates at 1 km-intervals along the array and secondly integrating horizontally to obtain T_{net} and T_{sw} (Figure 3.4).

3.5 Comparison of the transport proxy to actual model transports

The HYCOM proxy should ideally have a strong relationship with the simulated HYCOM transport. Both transports were computed from the same model simulation over the same region, and the transport calculation methods were consistent. The only differences between the transport calculation methods was that the HYCOM proxy estimated the transport based on the independent sea surface slope and the simulated model transport was calculated using the full-depth velocity field across the array. The correlations and transport statistics between the model and proxy provided insight to processes the proxy may have failed to represent, which were further investigated using HYCOM fields.

Based on the results obtained from the correlations between the proxy and model transports

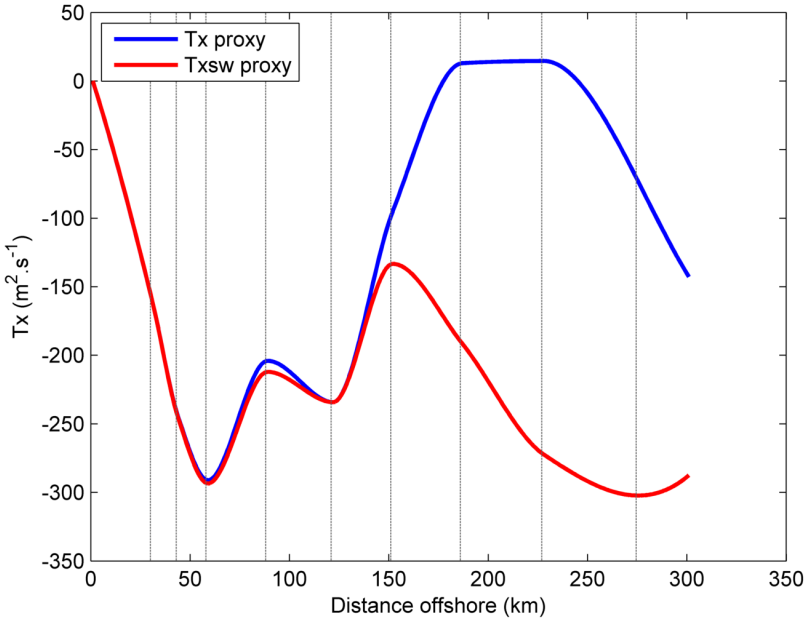

Figure 3.4: HYCOM transport per unit distance proxy ($m^2.s^{-1}$) for the net (blue) and southwest transport (red) at 1km intervals at the first model timestep. Grey lines represent the moorings and offshore CPIE pairs.

(see section 4.1 and 4.2) it was evident that the transport proxy was more capable of estimating the net transport rather than the southwest transport component only (Figure 4.1 and Table 4.1), hence further analysis mainly focused on the net transport proxy (T_{net}). The strengths and weaknesses of the net proxy were further investigated by selecting the highest and lowest correlated years from the 34-year annual correlation (Figure 4.2), and evaluated by plotting the current structure in the model over the respective years (Figures 4.3-4.5). Eddy kinetic energy (EKE) was calculated to show the surface variability of the current coincident with averaged SSH contours used to represent the mean surface structure (Figure 4.3). The eddy kinetic energy was calculated as follows:

$$EKE = \frac{\overline{(u')^2} + \overline{(v')^2}}{2} \tag{3.1}$$

where u' and v' are the zonal and meridional time-varying geostrophic current components respectively. In order to evaluate the subsurface current structure along the ACT array, the cross-track velocity at each depth layer in HYCOM was extracted in 12 km intervals from 0km to 400 km offshore, for the 34-year model period. Although the ACT array only extended to 300 km offshore, it was tempting to evaluate the current structure beyond the end of the array. Previous analyses have shown increased levels of offshore variability in this HYCOM simulation [Backeberg et al., 2009; 2014], which therefore made it interesting to observe the subsurface

structure during the offshore current meanders and the influence these could have on the transport proxy. The subsurface structure of the current was evaluated by investigating the average cross-track velocity for the highest and lowest correlated years and cross-track anomaly plots were used to understand the differences between the subsurface structure during the highest and lowest correlated years to the 3-year development period.

3.6 Sensitivity tests

To test the sensitivity of the time span of observations used to create the transport proxy, sensitivity experiments were performed to test how many years of virtual *in situ* observations are needed to create an accurate proxy to monitor the Agulhas Current transport. Using 34 years of model data the linear relationship could be tested over much longer or shorter periods.

Using the method described in section 3.4.3, regression models were built for 1, 6, 12, 18 and 34 years respectively. In addition, the linear relationship was calculated over two random 3-year periods, to test the influence that different current dynamics over different years could have on the development of the transport proxy. Lastly, the linear relationship was calculated over the maximum and minimum annual transport years in HYCOM, as well as during the years the HYCOM transport standard deviation was the largest and the smallest. This could test the dependence of the transport proxy on the accuracy of the transport estimate simulated in HYCOM. Although, the analysis of the proxy is focused on the net transport, it was interesting to test the development of the southwest transport proxy to the same time periods (Appendix, Figure A2 and Table A1).

Table 3.3: Sensitivity experiment time periods.

Time range (years)	**Model dates**
1	3 Jan 2011 - 27 Dec 2011
3	20 Apr 2010 - 18 Feb 2013
6	3 Jan 2009 - 19 Dec 2014
12	3 Jan 2003 - 19 Dec 2014
18	3 Jan 1997 - 19 Dec 2014
34	3 Jan 1980 - 19 Dec 2014
3*	3 Jan 1980 - 27 Dec 1982; 3 Jan 2000 - 27 Dec 2002
Max (Min) HYCOM transport.	2003 (1982)
Max (Min) HYCOM transport STD.	2013 (1980)

3* Corresponds to the random 3-year periods

Table 3.3 shows the time range over which the sensitivity experiments were performed. The

starting date, the 3rd of January, corresponds to the 1st week of each year based on the HYCOM time sequence and the 19th of December corresponds to the last week in the 34-year simulation. The 3-year *in situ* period in the model corresponded to the actual time range over which the *in situ* experiment was conducted, 15 April 2010- 19 February 2013 [Beal et al., 2015].

Calculating the transport proxy over a range of time periods, could therefore indicate how dependent it is on the current dynamics in the model and whether the dynamics may have changed over the different time periods. The following chapter 4, will present the results of the model transport proxy in attempting to address the study objectives outlined in section 1.1.

Chapter 4

Results

4.1 Proxy validation

In order to test the accuracy of the net and southwest HYCOM transport proxies they were compared to the net and southwest transports extracted from HYCOM (as described in section 3.5). This aided the investigation in terms of identifying transport events or features the proxy failed to represent.

Correlating the 3-year proxy transport (2010-2013) to the model transport over the same period, the net transport proxy explained 57% of the variance (R^2=0.57) while the southwest transport proxy only explained 14% of the variance (R^2=0.14). Assuming a constant three-year linear relationship for the nine regression models, the transport proxy was extended using 34-years of HYCOM SSH slope, after which the 34-year net transport proxy explained 52% of the variance (R^2=0.52) and the southwest transport proxy explained 26% of the variance (R^2=0.26) (Figure 4.1). Results from the *in situ* proxy experiment by Beal and Elipot [2016] also showed that the net proxy (T_{box}) explained a higher percentage of variance, 61% (R^2=0.61), compared to the southwest transport proxy (T_{jet}), 55% (R^2=0.55), over the 22-year time series [Beal and Elipot, 2016].

Table 4.1 summarises the transport statistics based on the 3-year and extended 34-year time period. The 34-year mean transport and standard deviation from HYCOM for the net and southwest transport was -84 ± 47 Sv and -110 ± 38 Sv respectively. Based on the proxy the net transport was -87 ± 34 Sv and southwest transport -92 ± 31 Sv. A higher southwest transport was expected considering it excludes northeast counter-flows that decrease the total transport

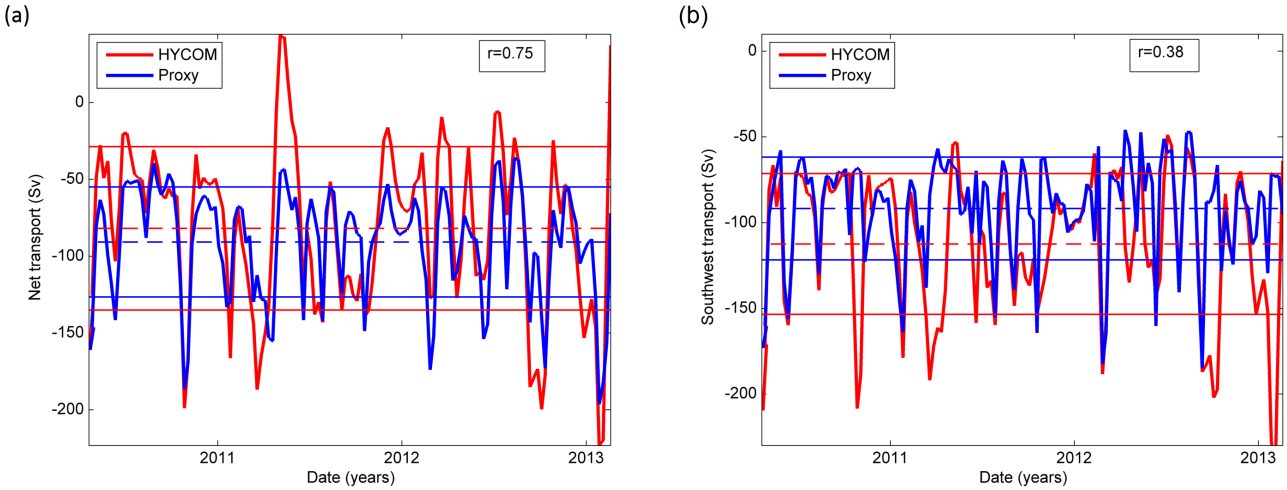

Figure 4.1: Transport time-series from the HYCOM proxy (blue) and the actual HYCOM transport (red). a & b for the 3-year correlation for the net and southwest transport respectively. The dashed horizontal lines represent the mean and the full horizontal lines represent the standard deviation, again blue (proxy) and red (HYCOM). Correlation coeficients are displayed in the top right corner.

Table 4.1: Summary of the transport statistics of the HYCOM model transport against the HYCOM proxy transport over the 3-year and extended 34-year time period. Negative values denote transport in the southwest direction. 1 Sv=10^6 m^3s^{-1}. Bold values represent the southwest transport results. Correlations are between the HYCOM model transport and HYCOM proxy transport, for the net transport (normal text) and southwest transport (bold text). All correlations were significant with 95% confidence.

	HYCOM (2010-2013)		**Proxy**		**HYCOM (1980-2014)**		**Proxy**	
Transport	T_{net}	$\boldsymbol{T_{sw}}$	T_{net}	$\boldsymbol{T_{sw}}$	T_{net}	$\boldsymbol{T_{sw}}$	T_{net}	$\boldsymbol{T_{sw}}$
Mean & Std (Sv)	-81 ± 53	**-112 ± 41**	-91 ± 35	**-92 ± 30**	-84 ± 47	**-110 ± 38**	-87 ± 34	**-92 ± 32**
Max (Sv)	-223	**-244**	-196	**-185**	-236	**-245**	-213	**-219**
Min (Sv)	44	**-48**	-36	**-46**	87	**-30**	-20	**-27**
r	0.75		**0.38**		0.72		**0.51**	

[Beal et al., 2015]. The differences between the standard deviations between HYCOM and the proxy indicates that transport in HYCOM experiences more variability compared to the proxy. The proxies only capture a portion of the transport estimate from the HYCOM model, suggesting it also only captures a portion of the model variability.

Figure 4.2 shows the annual correlations for the 34-year net and southwest transport time series. It is apparent that the southwest transport experiences much larger annual fluctuations in correlation to the HYCOM transport, having a significant maximum correlation of 0.818 (2014) and an insignificant minimum correlation of 0.002 (2003) (significance at 95% confidence interval).

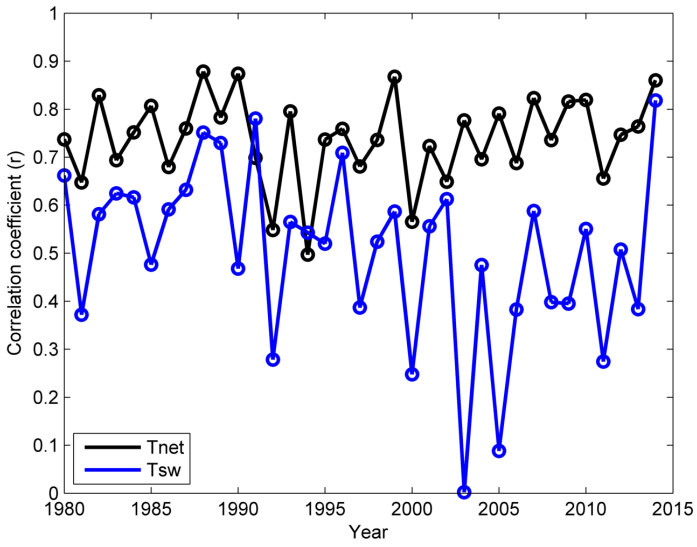

Figure 4.2: 34-year annual correlations between the net (black) and southwest (blue) transport proxy against the net and southwest transport extracted from HYCOM.

The annual correlations for the net transport were all significant with a maximum correlation of 0.88 (1988) and minimum correlation of 0.50 (1994). The net transport appears to have higher correlations for most of the 34-year time period, except during the years 1991 and 1994, where the southwest transport proxy has a higher correlation, 0.78 against 0.70 during 1991 and 0.54 against 0.50 during 1994. In summary, the results indicate that the proxy is generally better suited to estimate the net transport rather than the southwest transport component. Further analysis in this study therefore only focuses on the net transport component.

4.2 Evaluating the net transport proxy

The 34-year HYCOM output serves to evaluate the strengths and weaknesses of the net transport proxy by providing model output data needed to investigate the full-depth current structure as well as surface variability over the time period of the transport proxy. Investigating the full-depth current structure could emphasize important sub-surface processes which may not have distinct signatures at the surface and may therefore be excluded in the transport proxy.

The eddy kinetic energy plots (Figure 4.3 a & c) show the surface variability as well as the mean surface structure represented by the overlaying SSH contours for the highest (1988) and lowest (1994) correlated years of the net transport proxy. The mean EKE is higher across and downstream of the array during 1988, when the correlation is high, with a relatively stable current structure in comparison to 1994, where the EKE is lower and the current appears to be

meandering offshore. The narrow spacing of the SSH contours for both years indicates a strong gradient inshore and hence a strong mean geostrophic current, however the wide spacing between the SSH contours offshore suggests that the variability in the model is confined to the offshore side of the current.

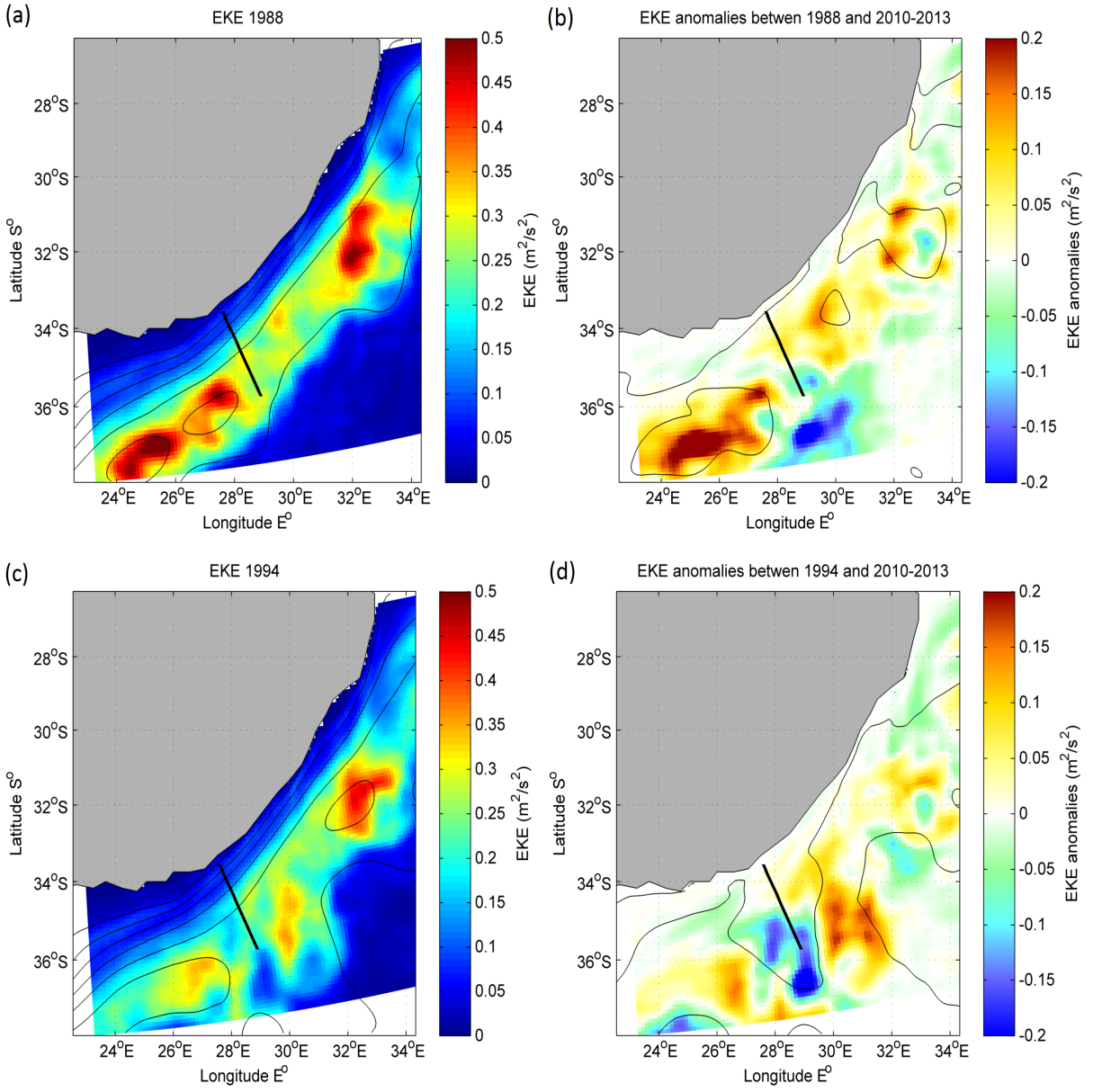

Figure 4.3: Mean eddy kinetic energy (EKE in m^2s^{-2}) and sea surface height (SSH in m) contours during (a) the highest (1988) and (c) lowest (1994) correlated years. b) EKE and SSH anomalies between 1988 and the development period (2010-2013) and (d) between 1994 and 2010-2013. The black line representing the ACT array.

The EKE anomaly plots (Figure 4.3b & d) show the difference between the mean EKE and SSH from the years used to develop the proxy (2010-2013) and the highest and lowest correlated years, 1988 and 1994 respectively. Results indicate that the current variability during 1988 was

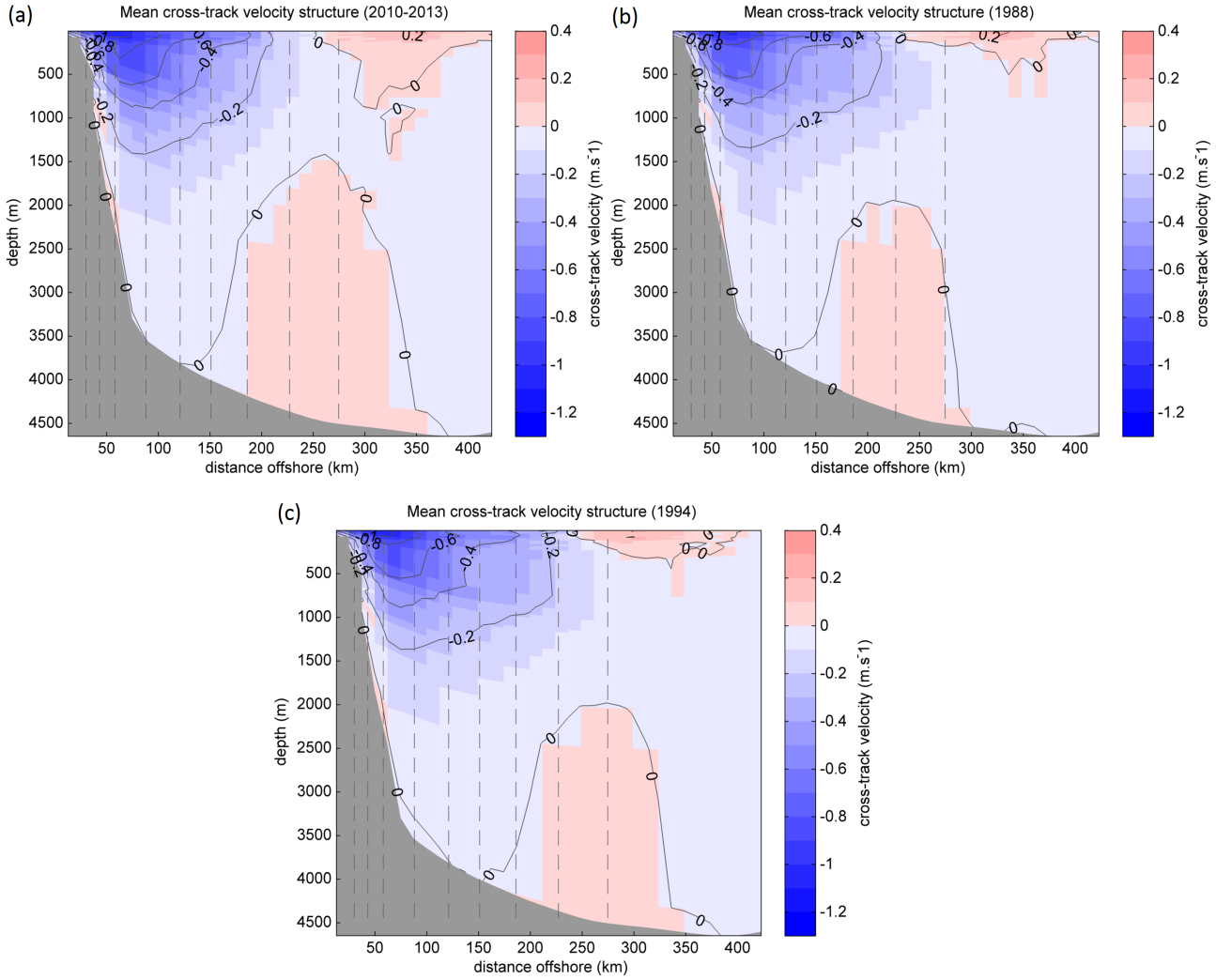

Figure 4.4: Mean cross-track velocity (m s^{-1}) structure during (a) the 3-year development period (2010-2013), (b) during the highest correlated year (1988) and (c) the lowest correlated year (1994). Blue shading represents the negative southwest direction and pink represents positive northeast. Contours are every 0.2 m s^{-1}. Dashed vertical lines represents the nine locations of the mooring and CPIES pairs.

similar to the current variability across the ACT array during the 3-year development period (2010-2013), thus showing a small difference in terms of the mean EKE. Whereas, the lowest correlated year (1994) experienced less variability across the array but higher levels of variability offshore thus resulting in the offshore, meandering mean structure. Table 3.2, highlighted that the performance of the offshore proxies (mooring G, P3P4 and P4P5) were poorer than the inshore proxies ($R^2 < 0.60$) which also suggests that less variance is explained by the proxy when the current is in a meandering state.

Figure 4.4 shows the mean cross-track velocity structure during the proxy development period (2010-2013), the highest correlated year (1988) and the lowest correlated year (1994). The mean

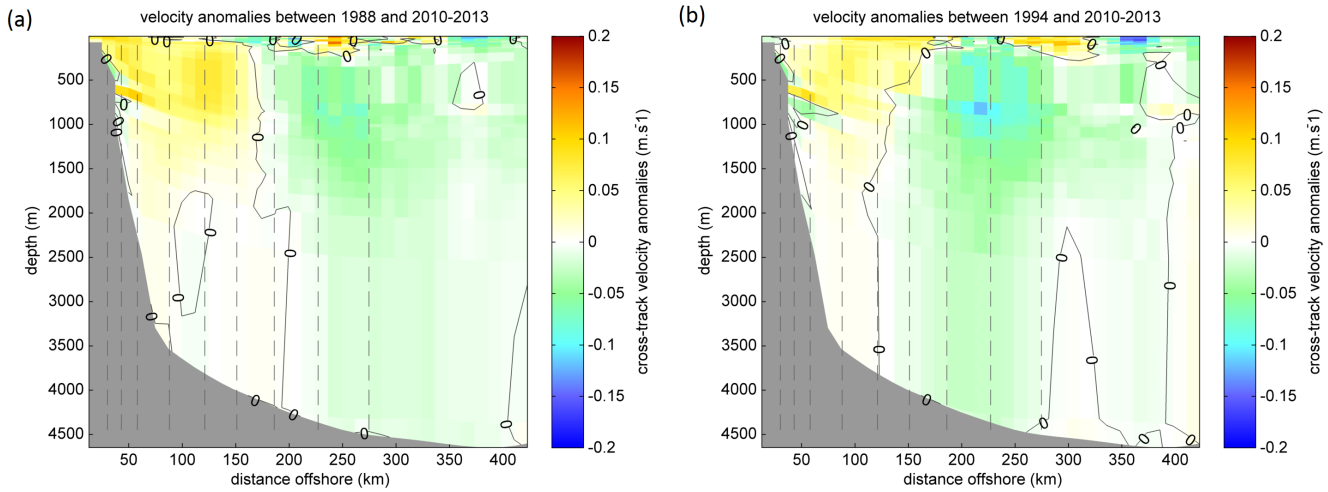

Figure 4.5: Cross-track velocity anomalies (m s^{-1}) between the mean cross-track velocity during (a) the highest correlated year (1988) minus the mean cross-track velocity over the development period (2010-2013), (b) as for (a) but between the lowest correlated year (1994). Dashed vertical lines represents the nine locations of the mooring and CPIES pairs.

position of the zero isotach indicates the vertical and horizontal extent of the current. For all three periods the current appears to extend full-depth inshore and offshore, except for the presence of the northeast counter flow, 200 km offshore, extending from a depth of 2000 m to the seafloor. Lastly, the horizontal extent of the zero isotach reveals that the current is shifted slightly offshore during 1994.

The cross-track velocity anomaly plots (Figure 4.5) highlight the differences between the mean cross-track velocity structure during the development period and the highest and lowest correlated years. Although the differences are very small, the current appears to be stronger by ∼5-10% inshore (mooring pairs A-F) and at the surface up to the last CPIES-pair P4P5 during the development period, whereas the current is ∼5% stronger offshore (G, P3-P4, P4-P5) during 1988 and ∼5-10% stronger offshore during 1994. There is also more subsurface current variability offshore in 1994. These small differences in the cross-track structure are therefore not the main factors resulting in the maximum and minimum correlations.

To gain further insight on the current structure during the highest and lowest correlated years the annual transports were investigated. The results obtained showed that the mean transport during the highest and lowest correlated years were equivalent (Figure not shown). The mean transport and standard deviation during the highest correlated year (1988) as estimated by the proxy was -85 ± 37 Sv against the lowest correlated year (1994) which estimated -85 ± 28 Sv. During the same years HYCOM estimated a mean transport of -72 ± 39 Sv (1988) and -90 ± 27

Sv (1994) respectively. The result are difficult to interpret using annual means, thus calculating the proxy over 1 year and viewing individual transport events provided clearer results (See section 4.4).

4.3 Sensitivity tests

The discussion of the 34-year Agulhas transport proxy throughout the investigation was thus far based on a 3-year (2010-2013) linear relationship between transport and SSH slope. The statistics summarized in Table 4.2 and Figure 4.6 illustrates the results obtained from calculating the linear relationship between transport and SSH slope over 1, 3, 6, 12, 18 and 34 years. The proxy transport was thereafter obtained by extending each linear relationship to the entire model time period and compared against the 34-year HYCOM transport. The taylor diagram therefore represents the spatial distribution of the results in terms of standard deviation, correlation and root-mean-squared-error (RMSE). The correlation coefficient based on the initial 3-year linear relationship was 0.72, however figure 4.6 shows that calculating the proxy over longer time periods did not improve the correlation or the RMSE. Calculating the proxy over 1 year decreased the correlation by only 1%. The only visible difference was the decrease in standard deviation. This was a surprising result, as it was expected that the correlation and standard deviation would increase, and the RMSE would decrease to correspond to the model transport estimates. The sensitivity of the net transport proxy was also tested using two random 3-year development periods. In comparison to the correlation obtained during 2010-2013 the correlation decreased by 2% during 1980-1982 and remained that same during 2000-2002. The results obtained from calculating the net proxy during the maximum (minimum) transport and standard deviation years in HYCOM showed no improvement or decrease in the skill of the proxy suggesting that the proxy is not directly impacted by the accuracy of the transport estimate simulated by HYCOM (results not included).

Table 4.2: Transport statistics and correlation results obtained from calculating the net transport proxy over a range of time periods.

Net transport	Transport (Sv)	STD (Sv)	RMSE (Sv)	r
MODEL	-84.32	47.23	0	1.00
1-yr	-87.26	35.47	33.36	0.71
3-yr	-87.21	34.09	32.76	0.72
6-yr	-87.04	35.91	33.04	0.72
12-yr	-86.91	32.51	32.83	0.72
18-yr	-88.71	31.28	32.95	0.72
34-yr	-88.15	29.74	33.14	0.72
1980-1982	-87.86	26.80	34.14	0.70
2000-2002	-94.80	30.31	32.87	0.72

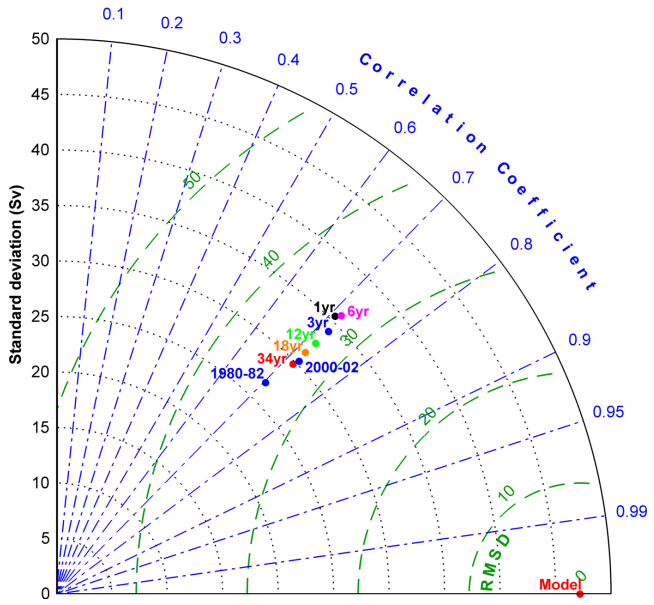

Figure 4.6: Taylor diagram showing the results of the net transport proxy calculated based on a 1-year linear relationship (black), 3-years (blue), 6-years (magenta), 12-years (green), 18-years (orange), 34-years (red) and during 1980-1982 and 2000-2002 (blue).

4.4 Investigating the transport variability

Previous analysis on the surface and cross-track velocity structure of the current was based on the annual means from the highest and lowest correlated years during the 34-year transport time-series (Figures 4.3-4.5). This made it difficult to interpret individual transport events that the proxy may have failed to represent, therefore analysing the proxy over 1-year made it easier to investigate the current structure corresponding to individual transport events (Figure 4.7). The year 2011 was selected for analysis as this was the 1-year period over which the transport proxy was developed during the sensitivity tests (Table 4.2 and Figure 4.6).

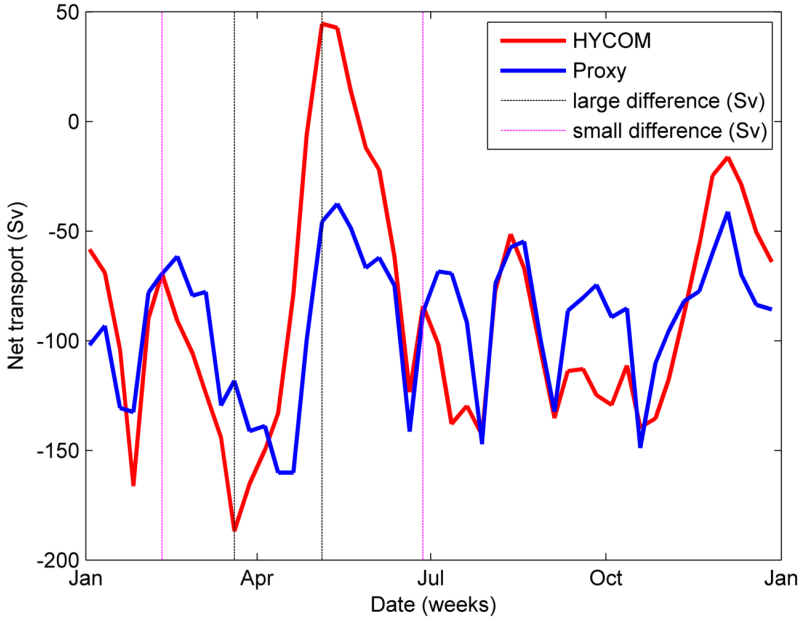

Figure 4.7: Weekly transport time-series during 2011, proxy in blue and HYCOM in red. Vertical lines correspond to the transport events where the transport estimates between HYCOM and the proxy were small, 10-February & 27-June (magenta) and large, 20-March & 5-May (grey).

The smallest differences between the HYCOM and proxy transport occurred during the week of the 10th of February 2011, where the proxy estimated -70 Sv and HYCOM -69 Sv and during the week of the 27th of June 2011, the proxy estimated -87 Sv and HYCOM -84 Sv (Figure 4.7). By plotting the surface geostrophic currents (Figure 4.8 a & b) it is apparent that the current is relatively stable on the inshore edge of the array during 10-February and relatively weak inshore with a strong anticyclonic eddy on the offshore edge of the array during 27-June. The cross-track velocity structure for both dates (Figure 4.8 c & d) reveal weak subsurface counter flows, however sub-surface velocities ranging between 0 - 0.2 m s^{-1} may not have an influence on the SSH at the surface or drastically change the transport of the water column.

Figure 4.9 represents the SSH across the array for the corresponding weeks with a small and large transport difference between the HYCOM proxy and HYCOM model transport. During the week of the 10th of February there is an increasing SSH slope over the inshore edge of the array, particularly across moorings A-D, thereafter the slope levels off to the end of the array. During the week of the 27th of June, a similar SSH slope is present at the inshore edge of the array or the region of the current core, but instead of levelling off up to the end of the array, the SSH slope increases again from mooring G up to the last CPIE-pair.

The largest transport differences between HYCOM and the proxy during 2011 occurred during

the week of the 20th of March where the proxy estimated -118 Sv and HYCOM estimated -186 Sv and during the week of the 5th of May with an estimate of -46 Sv and +45 Sv, for the proxy and HYCOM respectively (Figure 4.7). During the week of the 20th of March the current appears to be strong and narrow along the inshore edge of the array, with a strong anticyclonic eddy on the offshore edge (Figure 4.10). The current still displays an equivalent barotropic structure, that it holds even in the case of the impinging anticyclonic eddy. During the 5-May the entire current appears weaker, perhaps due to the extraction of kinetic energy from the mean flow by the downstream eddy.

Figure 4.9, displays the SSH slope during the weeks corresponding to the largest transport differences. During 20-March the current slope increases at the inshore edge of the array, in

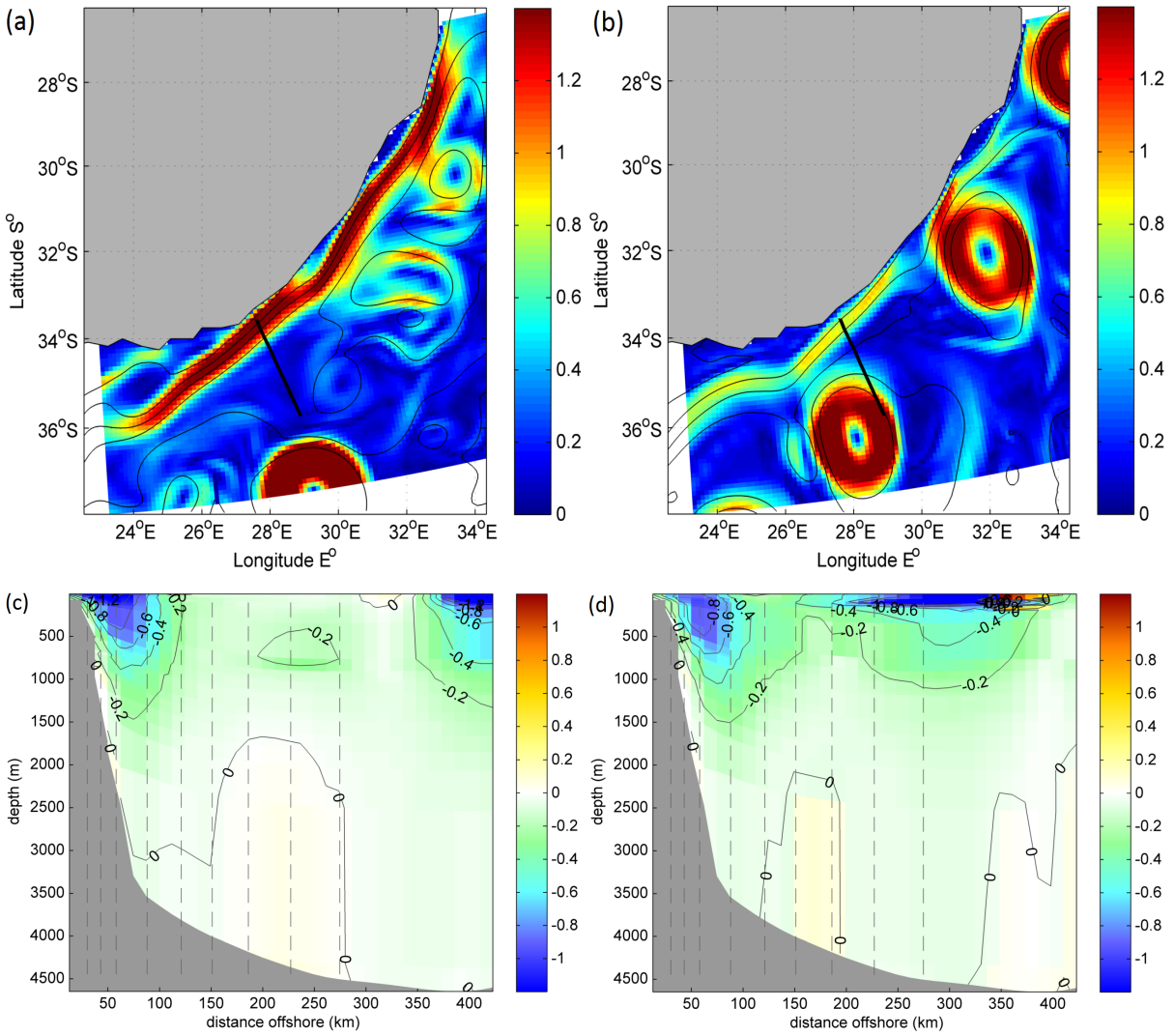

Figure 4.8: Surface geostrophic speed (m.s^{-1}) and SSH contours (m) during (a) 10-February and (b) 27-June. Cross-track velocity structure (m.s^{-1}) during (c) 10-February and (d) 27-June. Dashed lines represent the mooring and offshore CPIES-pairs.

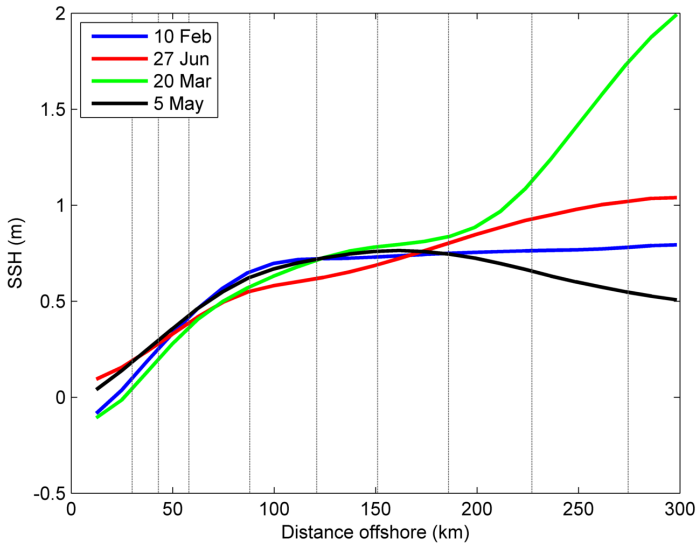

Figure 4.9: SSH (m) along the ACT array corresponding to the individual transport events under evaluation. Black dashed lines represent the positions of the ACT moorings (A-G & CPIES P3-P4 and P4-P5).

the vicinity of moorings A-D, from mooring D the slope levels off up to mooring G and then increases again up to the last CPIES-pair P4P5. This increase in SSH slope shows the steepest increase out of all the other transport events under investigation. The SSH during the 5-May displays a similar increasing slope at the inshore edge of the array up to mooring G, after which the SSH reveals a negative slope up to the end of the array, which is not observed during the other transport events.

The following chapter 5 will further discuss and summarise the results displayed in chapter 4, in an attempt to provide scientific evidence and to further substantiate the results with previous studies.

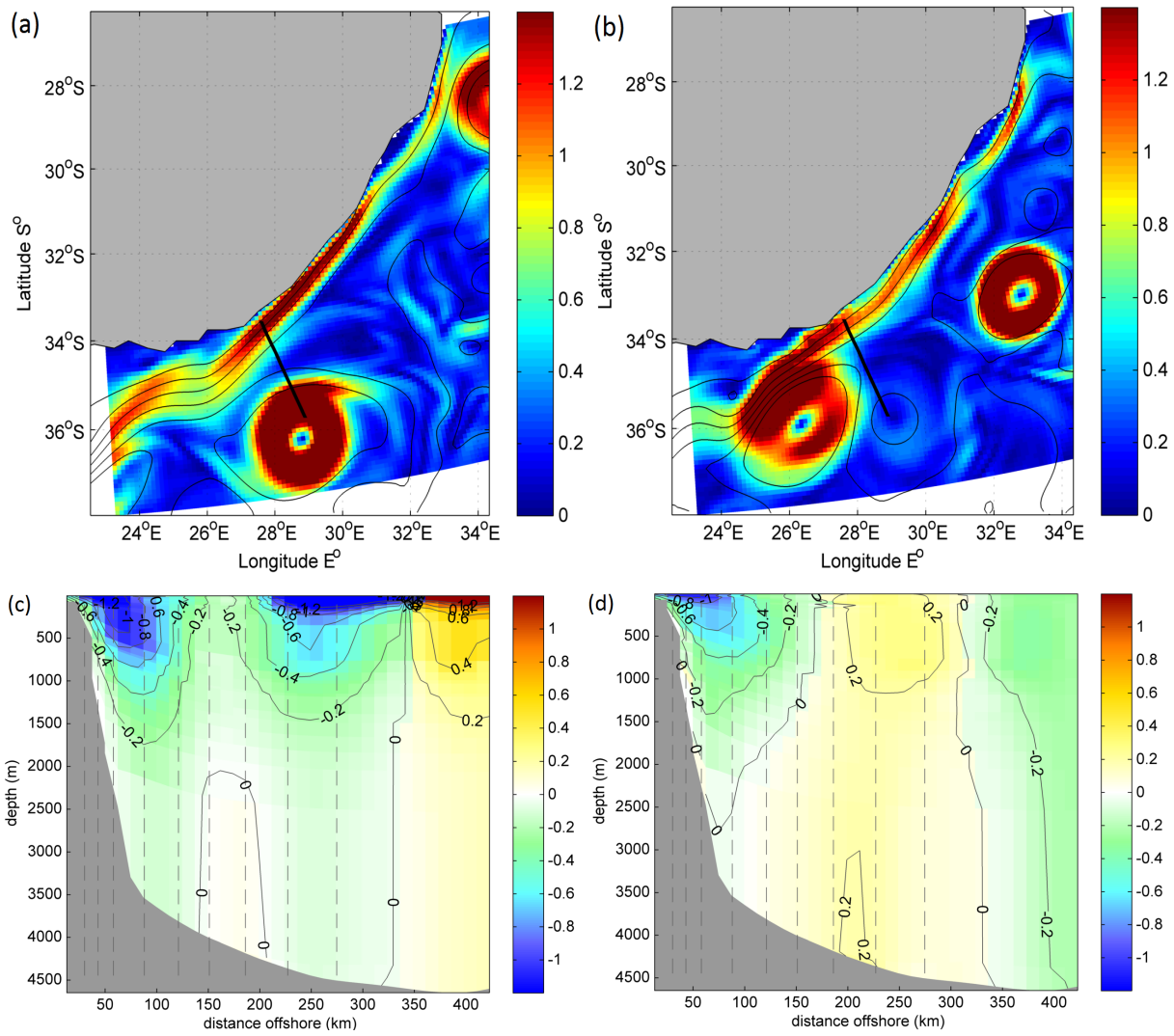

Figure 4.10: Surface geostrophic speed (m.s^{-1}) and SSH contours (m) during (a) 20-March and (b) 5-May. Cross-track velocity structure (m.s^{-1}) during (c) 20-March and (d) 5-May. Dashed lines represent the moorings and offshore CPIES-pairs.

Chapter 5

Summary

5.1 The Agulhas Current Transport Proxy

The Agulhas Current transport proxy, developed by Beal and Elipot [2016], was based on nine linear regression models, each assuming a three-year linear relationship between *in situ* transport and along-track sea surface slope measurements. Assuming nine constant linear relationships and a fixed three-year vertical current structure, the transport proxy was extended using 22-years of along-track satellite data spanning the years 1993-2015 from the TOPEX/Jason satellite mission [Beal and Elipot, 2016]. The Agulhas Current transport proxy in the current study replicates the methods used by Beal and Elipot [2016] but applies these using a regional HYCOM model of the Agulhas Current [Backeberg et al., 2009; 2014]. The HYCOM transport proxy was therefore developed using nine, three-year linear relationships between model transport and model SSH slope measurements, and extended using 34-years of the model SSH data from 1980 to 2014.

The HYCOM model provided the means to investigate the validity of the assumptions used to create the proxy, such as the fixed relationship between SSH slope and transport per unit depth at each mooring location and the length scale of observations needed to build a strong linear relationship between transport and SSH slope. In order to investigate the features the model proxy failed to observe, the transport time series estimated by the proxy was compared to the transport time series extracted from the model. The strengths and weaknesses of the transport proxy were further investigated using model velocity fields extracted across the virtual ACT array.

5.1.1 Proxy Validation

Two transport types, the net transport and the southwest transport component, were extracted from HYCOM in order to validate the net transport proxy (T_{net}) and the southwest transport proxy (T_{sw}). The T_{net} proxy explained a higher percentage of transport variance during the three-year period used to create the proxy (2010-2013), in comparison to the T_{sw} proxy, as well as during the extended 34-year period (1980-2014). However, the percentage of the explained transport variance of the T_{net} proxy decreased from 57% to 52% after using all 34-years of model data to build the linear proxy but increased from 14% to 26% for the T_{sw} proxy (Figure 4.1).

Results from Beal and Elipot [2016] also showed that the net transport proxy (T_{box}) explained a higher percentage of variance (61%) during the ACT period than the southwest transport proxy (T_{jet}: 55%). The performance, in terms of the measure of variance, of T_{net} in HYCOM was similar to the performance of the T_{box} proxy of Beal and Elipot [2016]. However, the T_{sw} proxy in HYCOM had a much lower performance. The difference in the performance of the model and *in situ* transport proxies, specifically the T_{sw} proxy, therefore suggests that HYCOM is unable to resolve all dynamics that occur in the Agulhas Current, particularly during meander events. Such model discrepancies include the consistent merging of the anticyclonic eddies with the Agulhas Current in the northern region [Backeberg et al., 2008], in addition to unresolved eddy dissipation in this region [Braby et al., 2016].

Figure 4.2 also shows that the T_{net} proxy explains more transport variance during the 34-year period in comparison to the T_{sw} proxy, except during the years 1991 and 1994. The poorer performance of the jet proxy could possibly be because it is only represents the southwestward flow, whereas the input sea surface slope reflects the net flow along the array. Interestingly, the T_{sw} proxy explained more transport variance during 1994, the same year T_{net} explained the least transport variance. Therefore, even though it appears the southwest transport proxy captured the current dynamics better during the years 1991 and 1994, the net proxy captured the current dynamics and hence estimated the transport with higher accuracy during the rest of the 34-year period, hence further analysis on the current structure was based on the net transport proxy only.

5.1.2 Evaluating the proxy performance

One of the main assumptions on which the Agulhas transport proxy relies is that the vertical stratification of the current does not change outside the 3-year development period [Beal and Elipot, 2016]. There are limitations to the albility of satellite altimeters to detect sub-surface variability [Robinson, 2004], however, in the Agulhas Current the vertical structure is equivalent barotropic, and this suggested that there is a strong relationship between SSH and full-depth transport [Elipot and Beal, 2015]. In this study, HYCOM was used to investigate the unexplained variance of the transport proxy in terms of horizontal and vertical variability.

The surface structure of the current was investigated in terms of the mean EKE and SSH contours (Figure 4.3), which are ideally equivalent to surface geostrophic flow and hence show the mean horizontal extent of the current [Robinson, 2004]. The vertical variability was investigated by plotting the mean cross-track velocity structure (Figure 4.4). Evaluating the annual mean surface and sub-surface structure would essentially dampen the signals of variability which were unexplained by the transport proxy, therefore the anomaly plots indicated the resemblance or differences of the current structure during the highest and lowest correlated years to the current structure during the development period (Figure 4.5).

During the highest correlated year (1988) the current is stable and inshore, whereas during the lowest correlated year (1994) the current is meandering and it appears that a large portion of the energy of the current has been shifted offshore, $>$ 300km. These results are consistent with Elipot and Beal [2015], showing that during the passage of a meander event, a large portion of kinetic energy is extracted from the flow through the process of barotropic conversion. Results from the analysis of the vertical structure of the current also showed that the current was shifted offshore during the lowest correlated year, however it indicated the offshore shift less clearly than the surface structure of the current, which is not a problem since the transport proxy is mainly able to capture the horizontal variability. Theoretically, the vertical structure of the velocity may be changed during current meander events [Zhu et al., 2004] but as was discussed, the signals of any distinct vertical changes were dampened in the mean representation of the current and is therefore analysed more closely in section 5.3.

The question still remains as to why most of the transport variance was explained in the year 1988 and the least in 1994? Table 3.2 highlighted that the performance of the linear regression models decreased offshore, suggesting that, when the current is in a meandering state, the net

proxy fails to accurately estimate the transport. It could be assumed that using the southwest transport proxy would improve the accuracy, however, the performance of the southwest regression models are only slightly stronger at the offshore end of the array. Therefore the HYCOM southwest transport proxy is less capable at capturing the transport when the Agulhas Current is in a meandering state. The southwest transport proxy by Beal and Elipot [2016] was developed to effectively estimate the transport of the Agulhas Current in the event of a mesoscale meander, which generally causes the current to manifest as a full-depth, surface intensified, cyclonic circulation out to 150km from the coast with anticyclonic circulation farther offshore [Elipot and Beal, 2015]. The Agulhas meanders in the HYCOM simulation occur in association with large anticyclonic eddies predominantly defined to the offshore edge of the current, with a narrow, southwest stream against the coast [Backeberg et al., 2009] or in some instances with an anticyclonic eddy across the entire length of the array. The resolution of HYCOM is able to capture the mesocale dynamics of eddies however, it fails to resolve the near-coastal features, such as the inshore, surface intensified cyclonic motion. This would require a finer resolution at the coast, in order to reveal smaller offshore displacements, ∼50km, associated with these meander events [Elipot and Beal, 2015]. Finally, the consistent merging of eddies in the HYCOM simulation makes it difficult to test the performance of the southwest transport proxy.

5.2 Sensitivity tests

In situ measurements are needed to set the transport proxy coefficients, but how many years of *in situ* observations would adequately capture the dynamics of the current and hence provide a strong foundation to build a linear relationship that is applicable to longer time periods?

The development of the ACT transport proxy was initially tested using a regional NEMO configuration in order to evaluate the potential of the altimeter proxy to monitor the multi-decadal transport of the Agulhas Current [van Sebille et al., 2010]. Using the numerical model, it was concluded that the correlation between the Agulhas Current transport and gradient in sea surface height was greater than r=0.78 for any three-year measuring period, and is therefore an adequate timescale to build an accurate transport proxy [van Sebille et al., 2010].

The HYCOM output in the current study was used to test the validity of the relationship between transport and SSH slope over a range of time periods. It was hypothesised that building the linear relationship over longer time periods, >3 years, would increase the skill of the transport proxy, since the linear relationship would be independent and perhaps capture more current dy-

namics over the longer periods of time. This hypothesis was proven incorrect. The performance of the transport proxy based on the a 1-year development period captured 50% of the transport variance and correlating the transport proxy over 3-years or more increased the explained transport variance by only 2% and decreased the standard deviation of the transport time-series by an insignificant quantity of ∼5 Sv over the 34-year period. Building the transport proxy over a different 3-year period over 1980-1982 explained 49% of the transport variance whereas over 2000-2002 the statistics remained 50% (Table 4.2 and Figure 4.6). This suggests that current dynamics for any 3-year period in the model could be very similar, as demonstrated by the error bars in Figure A1, and in agreement with the results obtained in van Sebille et al. [2010], which was encouraging since different models have different biases. The only differences between the two 3-year time periods may be the number of mesoscale meanders crossing the ACT array, which are discussed in the following section.

5.3 Investigating the transport variability in HYCOM

Previous studies have shown that the dominant mode of variability in the HYCOM simulation occurs in the form of large anticyclonic eddies, approximately 250-300 km in diameter, propagating southwestwards from the Mozambique Channel [Backeberg et al.,2008; 2009]. Weekly snapshots (Figures 4.8 and 4.10) reveal the presence of these mesoscale features and their influence on the vertical and horizontal extent of the Agulhas Current. The observation of mesoscale eddies requires that they produce a surface signature in the quantity being observed [Robinson, 2010]. In HYCOM these eddies do produce a strong surface signature as shown by the SSH contours in figures 4.8, 4.9 and 4.10 and should therefore be detected by the input SSH gradient in the transport proxy.

In order to investigate the influence that the anticyclonic features have on the transport proxy, the horizontal and vertical structure of the current was evaluated corresponding to the weeks where there was a significant difference between the HYCOM and proxy transport estimate. It is evident from figure 4.7 that the transport time series from the proxy does not correspond perfectly to the transport time series from HYCOM, in fact the transport proxy only explains 50% of the transport variance. During certain weeks the transport estimates are equivalent, such as during the weeks of 10-February and 27-June, but other weeks show a large difference between the proxy and HYCOM transport estimate, such as during 20-March and 5-May.

During the weeks of 10-February and 27-June 2011, the transport estimate predicted by the

proxy only differed by 1 Sv and 3 Sv respectively, in comparison to the transport estimated by HYCOM. During the 10-February the inshore current appears to be strong and stable along with the presence of an anticyclonic eddy far offshore, >350 km offshore (Figure 4.8 a & c) and during 27-June the inshore current is weaker with a large anticyclonic eddy across the offshore edge of the array ~250-300 km (Figure 4.8b & d). During the week of 20-March and 5-May 2011, the proxy transport estimate differed by 68 Sv and 91 Sv respectively. During both weeks, there was a narrow current flowing inshore against the coast with a strong anticyclonic eddy across the offshore edge of the array for the former and an anticyclonic eddy present downstream of the array for the latter (Figure 4.10).

As discussed, the presence of the anticyclonic eddies would be included in the transport proxy, but would the SSH slope be reflective of the transport beneath the eddy, are the eddies equivalent barotropic? Whilst evaluating the SSH slope it was important to consider the geostrophic approximation, stating that surface geostrophic currents are proportional to sea surface slope, where the steepness of the slope is equivalent to the intensification of the current speed [Stewart, 2008] and that a positive slope across the Agulhas Current corresponds to an increasing current speed and a negative slope corresponds to decreasing current speed.

At the inshore edge of the current, moorings A-C, revealed a positive SSH slope (Figure 4.9) and previous analyses have shown that the core of the current was found at moorings A,B and C for 90% of the time [Elipot and Beal, 2015]. Therefore, a positive slope relating to an increasing current speed was expected. During the week of 10-February the current appeared to have a constant surface speed to the end of the array, during 27-June and 20-March the current speed increased offshore, more so during 20-March and lastly, during the week of 5-May, the current speed decreased at the offshore edge of the array. These results are corroborated by figures 4.8 & 4.10 illustrating surface current geostrophic speed and SSH contours.

The influence of the mesoscale anticyclonic eddy during the week of 10-February would not have much of an impact on the transport proxy, since the mesoscale feature passes around the offshore edge of the array (Figure 4.8 a & c), however the impact of the anticyclonic eddies during the other three weeks needs to be considered carefully (Figures 4.8b & d and 4.10). The cross-track velocity structure beneath the anticyclonic eddies do reveal an equivalent barotropic structure, where the direction of the current velocity does not change with depth [Tsugawa and Hasumi, 2010; Lin and Che, 2012]. This is particularly visible in the cross-track current structure during

20-March 2011 (Figure 4.10c). This is satisfactory in the sense that the relationship between SSH slope and full-depth transport would remain strong during the passage of an anticyclonic eddy. The small, sub-surface variability observed inshore of the array, below 2000 m depth would not necessarily have a direct impact on the SSH signal or drastically change the volume transport of the water column. It has been observed in a layered ocean that, when assuming gesostrophy, the net transport in the uppermost layer is mainly proportional to the SSH slope [Andres et al., 2008].

It is important to consider that the Agulhas Current simulation in HYCOM is not completely realistic, demonstrating much higher levels of mesoscale variability than that normally observed [Backeberg et al., 2008; 2009]. Elipot and Beal [2015] recently showed that, on average, 1.6 mesoscale meanders pass through the ACT array at 34°S per year. In the HYCOM simulation an average of 5 anticyclonic eddies passed over the array per year. This was calculated by counting the weekly mesoscale eddies crossing the ACT array during certain years. This is in agreement with previous work [Backeberg et al., 2008] showing that the time-scale of eddies in the northern Agulhas Current is 5-6 times per year. A study by Braby et al. [2016] investigating eddy activity in the northern Agulhas Current using HYCOM, showed that both cyclonic and anticyclonic source eddies dissippate upon approaching the main Agulhas Current. However, the observed eddy interaction and dissipation process is poorly resolved in many numerical ocean models [Tsugawa and Hasumi, 2010; Durgadoo et al., 2013; Backeberg et al., 2014; Loveday et al., 2014], including the HYCOM model used in this study.

The frequently impinging eddies make it difficult to effectively estimate the accurate net transport of the Agulhas Current in the model since the advection of these eddies have previously been found to be responsible for the large transport fluctuations [Backeberg et al., 2009]. In some instances, such as during the week of 20-March 2011 only the inshore, southwestward edge of the eddy crosses the array causing the transport to spike. During other weeks, the entire eddy crosses the array, the southwest part on the inshore edge of the array and the northeast part on the offshore edge of the array. However, in such an event, if the eddies are symmetrical, there would be a cancellation between the southwest and northeast transport [Treguier et al., 2003] which would effectively remove the transport peaks.

The transport proxy therefore only includes the transport of the part of the eddy that is reflected in the SSH signal across the array, whether it is only the southwestward or northeastward portion

of the eddy or both, and should therefore match the transport peaks from the model. The transport in the model and proxy may fluctuate accordingly, however the transport estimates will not necessarily be equivalent, since it also depends on the strength of the proxy along the ACT array. In other words, the transport proxy may capture the SSH signal of the eddies along the array, however the correlation of the regression models decrease offshore, therefore transport estimates inshore would be more accurate than the transport estimates offshore when the current is in a meandering state.

Several studies have researched methods to decrease the levels of EKE in numerical simulations. Backeberg et al. [2009] improved the representation of the southern Agulhas Current by applying a higher-order momentum advection scheme, resulting in a well-defined meandering current rather than a continuous stream of eddies. Anderson et al. [2011] found that the use of relative wind forcing significantly decreased eddy intensities and a recent study [Renault et al., 2017 (in prep)] focussing on the current stress feedback between the ocean and atmosphere demonstrated a reduction of mesoscale activity by deflecting energy from the geostophic current to the atmosphere, showing that the indirect current feedback, improved the representation of the Agulhas Current. Improving the mesoscale variability in the HYCOM model could therefore yield better results for the transport proxy in the future. It was encouraging though that the results were similar to those obtained by van Sebille et al. [2010], suggesting that the results were consistent despite the model biases.

Chapter 6

Conclusions and Future Research

6.1 Conclusions

The development of satellite altimetry over time has improved methods to monitor ocean circulation considering the spatial and temporal limitations involved with *in-situ* monitoring or unresolved processes in numerical ocean models. *In-situ* data can provide valuable, accurate information throughout the water column, satellite altimetry can provide broad temporal and spatial data of the surface ocean, and numerical ocean models can provide valuable hindcasts or forcecasts, that can further be used to manipulate a system to improve our understanding of the underlying dynamics. Therefore, if one were to combine all three sampling methods, it could provide a very strong monitoring system that could improve the application of these datasets in operational oceanography in the future and to monitor long-term variability of ocean currents in the changing climate.

The Agulhas Current Time-series (ACT) experiment provides a clear example of a study that has employed *in situ*, satellite altimetry and numerical modelling data in order to capture the strength and variability of the Agulhas Current System. The experimental set up of the ACT mooring array and the underling hypotheses of the ACT proxy were initially tested using a numerical ocean model as is discussed in van Sebille et al. [2010]. Shortly after, the ACT mooring array was set up perpendicular to the south-east coast of South Africa, ~34°S, positioning it directly beneath the TOPEX/Poseidon-Jason altimeter ground track #96. These observations were used to derive a volume transport of the current that also captured transport variations during meander events [Beal et al., 2015]. Finally, the observations were used in combination with the

T/P-Jason satellite data in order to characterise mesoscale variability in the current [Elipot and Beal, 2015] and lastly, to build a 22-year time-series of Agulhas Current transports [Beal and Elipot, 2016].

The purpose of this modelling study was to re-create the Agulhas Current transport proxy in a virtual modelling environment, to test the validity of the underlying assumption on which the satellite-altimeter proxy was based. The Agulhas transport proxy developed by Beal and Elipot [2016] assumed nine, constant linear relationships between SSH slope and integrated transport per unit distance over the 22-year transport time-series, based on the 3-year sampling period and a constant vertical stratification. In other words, ignoring changes that could potentially influence the vertical structure of the current and hence violate the assumption of the constant linear relationship. The 34-year regional-hindcast from HYCOM provided the means to test the sensitivity of the transport proxy to vertical changes in the current and the length scale of observations used to build a strong, constant, linear relationship between transport and SSH slope.

Throughout the investigation it was found that HYCOM contained exaggerated levels of variability offshore of the Agulhas Current. The correlations of the regression models were stronger inshore and weaker offshore, as opposed to the results from the *in-situ* study [Beal and Elipot, 2016], where the performance of the inshore regression models were weaker inshore and stronger offshore. It was concluded that the poor performance of the inshore regression models during the *in-situ* study could possibly be due to the strongly sloping seabed and presence of the Agulhas Undercurrent [Beal and Elipot, 2016], whereas in HYCOM the poor performance of the offshore regression models were due to the exaggerated levels of offshore variability [Backeberg et al., 2014]. The development of the southwest transport proxy, which was developed to specifically capture the Agulhas Current transport during offshore meander events [Beal et al., 2015], did not significantly improve the performance of the offshore regression models in HYCOM. Based on the overall performance of the 34-year transport proxies it was concluded that the proxy was more capable of estimating the net transport of the Agulhas Current across the array instead of only the southwest transport component in agreement to the results obtained in [Beal and Elipot, 2016]. This suggests that the poor performance of the southwest transport proxy may not necessarily be as a result of the exaggerated offshore variability but some other process which may also have resulted in a poorer skill during the *in situ* study. However, due to the poorer skill of the southwest transport proxy, the current variability was mainly investigated based on

the results of the net transport proxy only.

During the year of the highest correlation between the HYCOM proxy transport and HYCOM model transport the current appeared to be stable and inshore whereas, during the lowest correlated year the current appeared to be in a meandering state, far offshore. This suggested that the transport associated with a meandering current was poorly estimated due to the poor performance of the offshore regression models. The net transport proxy was able to capture a portion of the transport variance during the passage of the anticyclonic eddies, since they do not breakdown the assumption of an equivalent barotropic structure and produced a clear surface signature in the SSH across the array. The transport in the model and the proxy therefore fluctuates accordingly, however the transport estimates will differ based on the mean position of the current along the array and therefore the strength of the regression models corresponding to the position on the array.

Testing the validity of the relationship between transport and SSH slope, results showed that calculating the proxy over longer time periods did not improve the accuracy. This suggested that the current dynamics for any-three year period was very similar in the model, thereby justifying that 3-years was a sufficient time-period used to develop the satellite-altimeter transport proxy of the Agulhas Current in HYCOM. The main conclusion drawn from this study is that the high levels of offshore variability resulted in the poor performance of the offshore linear regression models. This resulted in a poor estimation of the Agulhas Current transport when the current is in a meandering state, and perhaps a weaker performance of the southwest transport proxy.

6.2 Future Research

Numerical ocean models need to be capable of resolving the mesoscale dynamics and variability of the greater Agulhas Current in order to be considered of use in an operational oceanography system. It is important to note that the Agulhas Current does not experience such high levels of mesoscale variability as was illustrated in this regional HYCOM simulation and that this is a common error in many other ocean models of the region [eg. Durgadoo et al., 2013; Backeberg et al., 2014; Loveday et al., 2014]. Decreasing levels of mesoscale variability, by improving the eddy dissipation schemes, correcting the current stress feedback between the ocean and atmosphere [Renault et al., 2016], or adjusting the model to accurately resolve the near shore dynamics involved during Agulhas meanders, could eventually yield better results for the transport proxy in the future.

This study showed that calculating the linear relationship between SSH slope and transport based on weekly time periods, longer than three years, did not significantly improve the skill of the Agulhas transport proxy. To further test the optimal sampling rate in HYCOM, instead of using the weekly model output, the transport proxy could be developed using a daily HYCOM product. Using daily data one can test the sensitivity of the proxy to sampling frequency, e.g. daily, 3-day, 10-day or longer. Sensitivity studies of this kind, using numerical ocean models, could provide useful information into planning *in situ* studies in the future, and understanding the sensitivities and limitations of transport proxies could further improve long-term monitoring methods in the global ocean.

Bibliography

Anderson, L. A., McGillicuddy, D. J., Maltrud, M. E., Lima, I. D., and Doney, S. C. (2011). Impact of eddy-wind interaction on eddy demographics and phytoplankton community structure in a model of the North Atlantic Ocean. *Dynamics of Atmospheres and Oceans*, 52(1-2):80–94.

Andres, M., Park, J.-H., Wimbush, M., X-H, Z., Chang, K., and Ichikawa, H. (2008). Study of the Kuroshio / Ryukyu Current System Based on Satellite-Altimeter and in situ Measurements. *Journal of Oceanography*, 64:937–950.

Ansorge, I. J., Baringer, M. O., Campos, E. J. D., Dong, S., Fine, R. A., Garzoli, S. L., Goni, G., Meinen, C. S., Perez, R. C., Piola, A. R., Roberts, M. J., Speich, S., Sprintall, J., Terre, T., and Van Den Berg, M. A. (2014). Basin-wide oceanographic array bridges the South Atlantic. *EOS*, 95(6):53–54.

Antonov, J., Locarnini, R., Boyer, R., Mishonov, A., and Garcia, H. (2006). World ocean atlas 2005. 2, Salinity.

Backeberg, B. C., Bertino, L., and Johannessen, J. A. (2009). Evaluating two numerical advection schemes in HYCOM for eddy-resolving modelling of the Agulhas Current. *Ocean Science*, (5):173–190.

Backeberg, B. C., Counillon, F., Johannessen, J. A., and Pujol, M.-I. (2014). Assimilating along-track sla data using the enoi in an eddy resolving model of the agulhas system. *Ocean Dynamics*, 64(8):1121–1136.

Backeberg, B. C., Johannessen, J. A., Bertino, L., and Reason, C. J. (2008). The greater Agulhas Current system: An integrated study of its mesoscale variability. *Journal of Physical Oceanography*, 1(1):29–44.

Ballegooyen, R. C., Gründlingh, M. L., and Lutjeharms, J. R. (1994). Eddy fluxes of heat and salt from the southwest indian ocean into the southeast atlantic ocean: A case study. *Journal of Geophysical Research: Oceans*, 99(C7):14053–14070.

Beal, L. and Bryden, H. (1997). Observations of an Agulhas Undercurrent. *Deep-Sea Research Part I*, 44(9):1715–1724.

Beal, L. M. (2009). A Time Series of Agulhas Undercurrent Transport. *Journal of Physical Oceanography*, 39(10):2436–2450.

Beal, L. M. and Bryden, H. L. (1999). The velocity and vorticity structure of the Agulhas Current at 32°S. *Journal of Geophysical Research*, 104(C3):5151.

Beal, L. M., De Ruijter, W. P. M., Biastoch, A., and Zahn, R. (2011). On the role of the Agulhas system in ocean circulation and climate. *Nature*, 472(7344):429–36.

Beal, L. M. and Elipot, S. (2016). Broadening not strengthening of the Agulhas Current since the early 1990s. *Nature Publishing Group*, 540(7634):570–573.

Beal, L. M., Elipot, S., Houk, A., and Leber, G. M. (2015). Capturing the Transport Variability of a Western Boundary Jet: Results from the Agulhas Current Time-Series Experiment (ACT). *Journal of Physical Oceanography*, 45(5):1302–1324.

Bernard, B., Madec, G., Penduff, T., Molines, J. M., Treguier, A. M., Le Sommer, J., Beckmann, A., Biastoch, A., Böning, C., Dengg, J., Derval, C., Durand, E., Gulev, S., Remy, E., Talandier, C., Theetten, S., Maltrud, M., McClean, J., and De Cuevas, B. (2006). Impact of partial steps and momentum advection schemes in a global ocean circulation model at eddy-permitting resolution. *Ocean Dynamics*, 56(5-6):543–567.

Biastoch, A. and Krauss, W. (1999). The Role of Mesoscale Eddies in the Source Regions of the Agulhas Current. *Jounrnal of Physical Oceanography*, 29:2303–2317.

Bleck, R. (2002). An oceanic general circulation model framed in hybrid isopycnic-cartesian coordinates. *Ocean modelling*, 4(1):55–88.

Braby, L., Backeberg, B. C., Ansorge, I., Roberts, M. J., Krug, M., and Reason, C. J. (2016). Observed eddy dissipation in the agulhas current. *Geophysical Research Letters*, 43(15):8143–8150.

Bryden, H., Beal, L., and Duncan, L. (2005). Structure and Transport of the Agulhas Current and Its Temporal Variability. *Journal of Oceanography*, 61(1980):479–492.

Cai, W. (2006). Antarctic ozone depletion causes an intensification of the Southern Ocean supergyre circulation. *Geophysical Research Letters*, 33(3):1–4.

Casal, T. G. D., Beal, L. M., Lumpkin, R., and Johns, W. E. (2009). Structure and downstream evolution of the Agulhas Current system during a quasi-synoptic survey in February-March 2003. *Journal of Geophysical Research: Oceans*, 114(3):1–16.

Chapron, B., Collard, F., and Ardhuin, F. (2005). Direct measurements of ocean surface velocity from space: Interpretation and validation. *Journal of Geophysical Research: Oceans*, 110(7):1–17.

Chassignet, E. P., Hurlburt, H. E., Smedstad, O. M., Halliwell, G. R., Hogan, P. J., Wallcraft, A. J., Baraille, R., and Bleck, R. (2007). The hycom (hybrid coordinate ocean model) data assimilative system. *Journal of Marine Systems*, 65(1):60–83.

Chelton, D. B., Deszoeke, R. A., Schlax, M. G., El Naggar, K., and Siwertz, N. (1998). Geographical variability of the first baroclinic rossby radius of deformation. *Journal of Physical Oceanography*, 28(3):433–460.

Cooper, K. (2014). Evaluating global ocean reanalysis systems for the greater agulhas current system. *Masters Thesis*.

de Ruijter, W. P. M., van Leeuwen, P. J., and Lutjeharms, J. R. E. (1999). Generation and Evolution of Natal Pulses: Solitary Meanders in the Agulhas Current. *Journal of Physical Oceanography*, 29(12):3043–3055.

Dee, D. P., Uppala, S., Simmons, A., Berrisford, P., Poli, P., Kobayashi, S., Andrae, U., Balmaseda, M., Balsamo, G., Bauer, P., et al. (2011). The era-interim reanalysis: Configuration and performance of the data assimilation system. *Quarterly Journal of the royal meteorological society*, 137(656):553–597.

Delworth, T. L., Clark, P. U., Holland, M., Johns, W. E., Kuhlbrodt, T., Lynch-Stieglitz, J., Morrill, C., Seager, R., Weaver, A. J., and Zhang, R. (2008). The Potential for Abrupt Change in the Atlantic Meridional Overturning Circulation. *Abrupt Climate Change*, pages 258–359.

Dijkstra, H. and de Ruijter, W. (2001). On the Physics of the Agulhas Current : Steady Retroflection Regimes. *Jounrnal of Physical Oceanography*, 31:2971–2985.

Durgadoo, J., Loveday, B., Reason, C., Penven, P., and Biastoch, A. (2013). Agulhas Leakage Predominantly Responds to the Southern Hemisphere Westerlies. *Jounrnal of Physical Oceanography*, 43:2113–2131.

Elipot, S. and Beal, L. (2015). Characteristics , Energetics , and Origins of Agulhas Current Meanders and their Limited Influence on Ring Shedding. *Journal of Physical Oceanography*, 45(9):2294—-2314.

Fu, L.-L., Chelton, D., Le Traon, P.-Y., and Morrow, R. (2010). Eddy Dynamics From Satellite Altimetry. *Oceanography*, 23(4):14–25.

George, M., Bertino, L., Johannessen, O., and Samuelsen, A. (2010). Validation of a hybrid coordinate ocean model for the indian ocean. *Journal of Operational Oceanography*, 3(2):25–38.

Gimeno, L., Drumond, A., Nieto, R., Trigo, R. M., and Stohl, A. (2010). On the origin of continental precipitation. *Geophysical Research Letters*, 37(13).

Gordon, A. L. (2003). Oceanography: The brawniest retroflection. *Nature*, 421(6926):904–905.

Gordon, A. L., Lutjeharms, J. R., and Gründlingh, M. L. (1987). Stratification and circulation at the Agulhas Retroflection. *Deep Sea Research Part A. Oceanographic Research Papers*, 34(4):565–599.

Gründlingh, M. L. (1980). On the volume transport of the agulhas current. *Deep Sea Research Part A. Oceanographic Research Papers*, 27(7):557–563.

Gründlingh, M. L. (1983). On the course of the agulhas current. *South African Geographical Journal*, 65(1):49–57.

Halo, I., Backeberg, B., Penven, P., Ansorge, I., Reason, C., and Ullgren, J. E. (2014). Deep-Sea Research II Eddy properties in the Mozambique Channel : A comparison between observations and two numerical ocean circulation models. *Deep-Sea Research Part II*, 100:38–53.

Hermes, J. C., Reason, C., and Lutjeharms, J. (2007). Modeling the Variability of the Greater Agulhas Current System. *Journal of climate*, 20(13):3131–3146.

I, A. and MJ, R. (2013). South african national antarctic programme (sanap). *Voyage Participation Details*.

Imawaki, S., Uchida, H., Ichikawa, H., and Fukasawa, M. (2001). Satellite altimeter monitoring the Kuroshio transport south of Japan. *Geophysical Research Letters*, 28(1):17–20.

Jury, M., Valentine, H., and Lutjeharms, J. (1993). Influence of the Agulhas Current on Summer Rainfall along the Southeast Coast of South Africa. *Journal of applied Meterology*, 32:1282–1287.

Krug, M. and Tournadre, J. (2012). Satellite observations of an annual cycle in the Agulhas Current. *Geophysical Research Letters*, 39(May):1–6.

Leber, G. M. and Beal, L. (2014). Evidence that Agulhas Current transport is maintained during a meander. *Journal of Geophysical Research: Oceans*, 119:3806–3817.

Lee, S.-K., Park, W., Van Sebille, E., Baringer, M. O., Wang, C., Enfield, D. B., Yeager, S. G., and Kirtman, B. P. (2011). What caused the significant increase in atlantic ocean heat content since the mid-20th century? *Geophysical Research Letters*, 38(17).

Lin, Z. and Che, S. (2012). A geostrophic empirical mode based on altimetric sea surface height. *Science China Earth Sciences*, 55(7):1193–1205.

Loveday, B. R., Durgadoo, J. V., Reason, C. J., Biastoch, A., and Penven, P. (2014). Decoupling of the agulhas leakage from the agulhas current. *Journal of Physical Oceanography*, 44(7):1776–1797.

Lutjeharms, J. and De Ruijter, W. (1996). The influence of the agulhas current on the adjacent coastal ocean: possible impacts of climate change. *Journal of Marine Systems*, 7(2-4):321–336.

Lutjeharms, J. R., Boebel, O., Vaart, P. C., Ruijter, W. P., Rossby, T., and Bryden, H. L. (2001). Evidence that the natal pulse involves the agulhas current to its full depth. *Geophysical research letters*, 28(18):3449–3452.

Lutjeharms, J. R. E. (2006). *The Agulhas Current*.

Lutjeharms, J. R. E. and Webb, D. J. (1995). Modelling the Agulhas current system with the Fne Resolution Antarctic Model (FRAM). *Deep-Sea Research*, 42(4):523–551.

Matano, R. P., Beier, E. J., Strub, P. T., and Tokmakian, R. (2002). Large-Scale Forcing of the Agulhas Variability: The Seasonal Cycle. *Journal of Physical Oceanography*, 32(4):1228–1241.

Maul, G. A., Mayer, D. A., and Bushnell, M. (1990). Statistical relationships between local sea level and weather with florida-bahamas cable and pegasus measurements of florida current volume transport. *Journal of Geophysical Research: Oceans*, 95(C3):3287–3296.

Nakamura, H. and Shimpo, A. (2004). Seasonal Variations in the Southern Hemisphere Storm Tracks and Jet Streams as Revealed in a Reanalysis Dataset. *Journal of climate*, 17:1828–1844.

Palastanga, V., Van Leeuwen, P., and De Ruijter, W. (2006). A link between low-frequency mesoscale eddy variability around madagascar and the large-scale indian ocean variability. *Journal of Geophysical Research: Oceans*, 111(C9).

Penven, P., Herbette, S., and Rouault, M. (2011). Ocean Modelling in the Agulhas Current System. In *Nansen-Tutu Conf Proc*, pages 17–21.

Reason, C. J. C. (2001). Subtropical Indian Ocean SST dipole events and southern African rainfall. *Geophysical Research Letters*, 28(11):2225–2227.

Reason, C. J. C. (2002). ENSO-like decadal variability and South African rainfall. 29(13):13–16.

Renault, L., Molemaker, M. J., Gula, J., Masson, S., and McWilliams, J. C. (2016). Control and stabilization of the gulf stream by oceanic current interaction with the atmosphere. *Journal of Physical Oceanography*, 46(11):3439–3453.

Ridderinkhof, H. and De Ruijter, W. P. M. (2003). Moored current observations in the Mozambique Channel. *Deep-Sea Research Part II: Topical Studies in Oceanography*, 50(12-13):1933–1955.

Roberts, M., Van der Lingen, C., Whittle, C., and Van den Berg, M. (2010). Shelf currents, lee-trapped and transient eddies on the inshore boundary of the agulhas current, south africa: their relevance to the kwazulu-natal sardine run. *African Journal of Marine Science*, 32(2):423–447.

Robinson, I. S. (2004). *Measuring the oceans from space: the principles and methods of satellite oceanography*. Springer Science & Business Media.

Robinson, I. S. (2010). *Discovering the ocean from space: The unique applications of satellite oceanography*. Springer Science & Business Media.

Rouault, M., Lee-Thorp, A., and Lutjeharms, J. (2000). The atmospheric boundary layer above the agulhas current during alongcurrent winds. *Journal of physical oceanography*, 30(1):40–50.

Rouault, M. and Lutjeharms, J. (2003). Estimation of sea-surface temperature around southern Africa from satellite-derived microwave observations. *South African journal of science*, 99(September/October):489–493.

Rouault, M., White, S. a., Reason, C. J. C., Lutjeharms, J. R. E., and Jobard, I. (2002). Ocean Atmosphere Interaction in the Agulhas Current Region and a South African Extreme Weather Event. *Weather and Forecasting*, 17(4):655–669.

Rouault, M. J., Mouche, A., Collard, F., Johannessen, J. A., and Chapron, B. (2010). Mapping the Agulhas Current from space : An assessment of ASAR surface current velocities. *Journal of Geophysical Research*, 115(December):1–14.

Rouault, M. J. and Penven, P. (2011). New perspectives on Natal Pulses from satellite observations. *Journal of Geophysical Research: Oceans*, 116(7):1–14.

Saenko, O. A., Fyfe, J. C., and England, M. H. (2005). On the response of the oceanic wind-driven circulation to atmospheric CO2 increase. *Climate Dynamics*, 25(4):415–426.

Sato, O. T. and Rossby, T. (1995). Seasonal and low frequency variations in dynamic height anomaly and transport of the Gulf Stream. *Deep-Sea Research Part I*, 42(1):149–164.

Schiller, A. and Brassington, G. B. (2011). *Operational oceanography in the 21st century*. Springer Science & Business Media.

Schouten, M. W., Ruijter, W. P. M. D., and Leeuwen, P. J. V. (2002). Upstream control of Agulhas Ring shedding. *Journal of Geophysical Research*, 107(C8).

Schumann, E. H. (1981). Low Frequency Fluctuations Off the Natal Coast. *Journal of Geophysical Research*, 86(1):6499–6508.

Siedler, G., Gould, J., and Church, J. A. (2001). *Ocean circulation and climate: observing and modelling the global ocean*, volume 103. Academic Press.

Siedler, G., Rouault, M., and Lutjeharms, J. R. (2006). Structure and origin of the subtropical South Indian Ocean Countercurrent. *Geophysical Research Letters*, 33(24):1–5.

Smith, L., , Boudra, D., and R, B. (1990). A Wind-Driven Isopycnic Coordinate Model of the North and Equatorial Atlantic Ocean 2 . The Atlantic Basin Experiments. *Journal of Geophysical Research*, 95:105–128.

Sprintall, J. and Revelard, A. (2014). The Indonesian Throughflow response to Indo-Pacific climate varaibility. *Journal of Geophysical Research: Oceans*, 119:1161–1175.

Stewart, R. H. (2008). *Introduction to physical oceanography*. Robert H. Stewart.

Stramma, L. and Lutjeharms, J. R. E. (1997). The flow field of the subtropical gyre of the South Indian Ocean. *Journal of geophysical research*, 102(C3):5513–5530.

Toole, J. M. and Warren, B. A. (1993). A hydrographic section across the subtropical south indian ocean. *Deep Sea Research Part I: Oceanographic Research Papers*, 40(10):1973–2019.

Treguier, A., Boebel, O., Barnier, B., and Madec, G. (2003). Agulhas eddy fluxes in a 1/6 degree Atlantic model. *Deep-Sea Research Part II*, 50:251–280.

Tsugawa, M. and Hasumi, H. (2010). Generation and Growth Mechanism of the Natal Pulse. *Jounrnal of Physical Oceanography*, 40:1597–1612.

Uppala, S. M., Kållberg, P., Simmons, A., Andrae, U., Bechtold, V. d., Fiorino, M., Gibson, J., Haseler, J., Hernandez, A., Kelly, G., et al. (2005). The era-40 re-analysis. *Quarterly Journal of the royal meteorological society*, 131(612):2961–3012.

van Sebille, E., Beal, L. M., and Biastoch, A. (2010). Sea surface slope as a proxy for Agulhas Current strength. *Geophysical Research Letters*, 37(9):2–5.

Walker, N. D. and Mey, R. D. (1988). Ocean/atmosphere heat fluxes within the agulhas retroflection region. *Journal of Geophysical Research: Oceans*, 93(C12):15473–15483.

Weijer, W., de Ruijter, W., and Dijkstr, H. (2001). Stability of the Atlantic Overturning Circulation : Competition between Bering Strait Freshwater Flux and Agulhas Heat and Salt Sources. *Jounrnal of Physical Oceanography*, 31:2285–2402.

Yan, X. and Sun, C. (2015a). An altimetric transport index for kuroshio inflow northeast of taiwan island. *Science China Earth Sciences*, 58(5):697–706.

Yan, X. M. and Sun, C. (2015b). An altimetric transport index for Kuroshio inflow northeast of Taiwan Island. *Science China Earth Sciences*, 58(5):697–706.

Yang, H., Lohmann, G., Wei, W., Dima, M., Ionita, M., and Liu, J. (2016). Intensification and poleward shift of subtropical western boundary currents in a warming climate. *Journal of Geophysical Research: Oceans*, 121:4928–4945.

Yang, Y., Liu, C., T, L., William, J., Li, H., and Koga, M. (2001). Sea surface slope as an estimator of the Kuroshio volume transport east of Taiwan. *Geophysical Research Letters*, 28(12):2461–2464.

Zhu, X. H., Ichikawa, H., Ichikawa, K., and Takeuchi, K. (2004). Volume transport variability southeast of Okinawa Island estimated from satellite altimeter data. *Journal of Oceanography*, 60(6):953–962.

Appendix

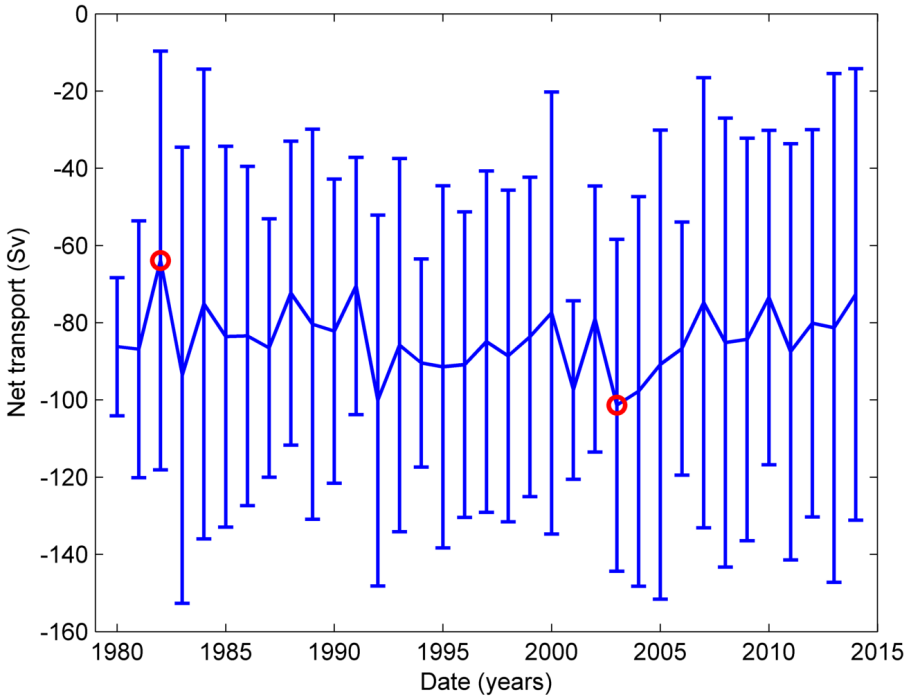

Figure A.1: HYCOM annual transport time series (T_{net}) with standard deviation error bars (± 1 STD). Maximum (2003) and minimum (1982) transport years encirciled in red.

Table A.1: Transport statistics and correlation results obatined from caluclating the southwest transport proxy over a range of time periods.

Southwest transport	Transport (Sv)	STD (Sv)	RMSE (Sv)	R
MODEL	-110.05	37.89	0	1.00
1-yr	-90.65	28.96	35.41	0.46
3-yr	-92.40	31.57	34.83	0.51
6-yr	-93.98	31.72	34.62	0.52
12-yr	-93.60	29.54	34.39	0.50
18-yr	-94.51	29.35	34.41	0.50
34-yr	-93.74	28.74	34.16	0.50
1980-1982	-92.82	26.45	33.26	0.51
2000-2002	-97.54	26.99	34.98	0.46

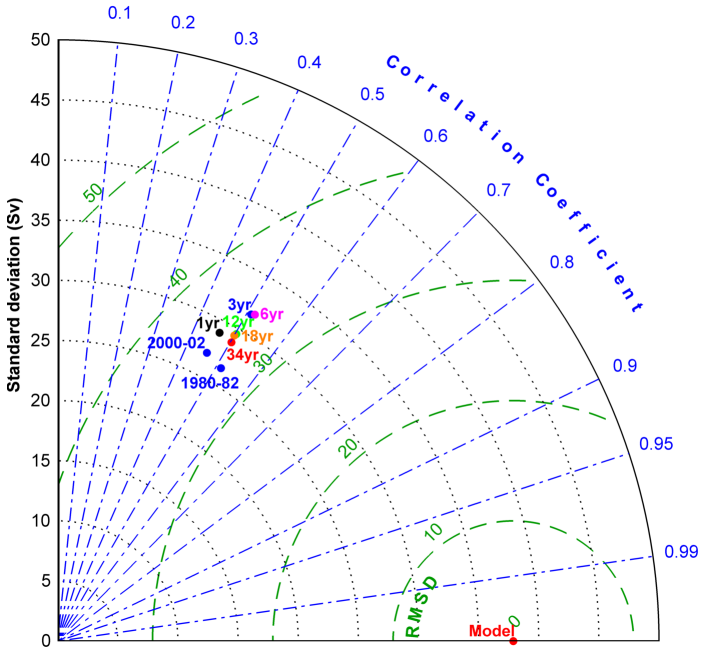

Figure A.2: Taylor diagram showing the results of the southwest transport proxy calculated based on a 1-year linear relationship (black), 3-years (blue), 6-years (magenta), 12-years (green), 18-years (orange), 34-years (red) and during 1980-82 and 2000-02 (blue).

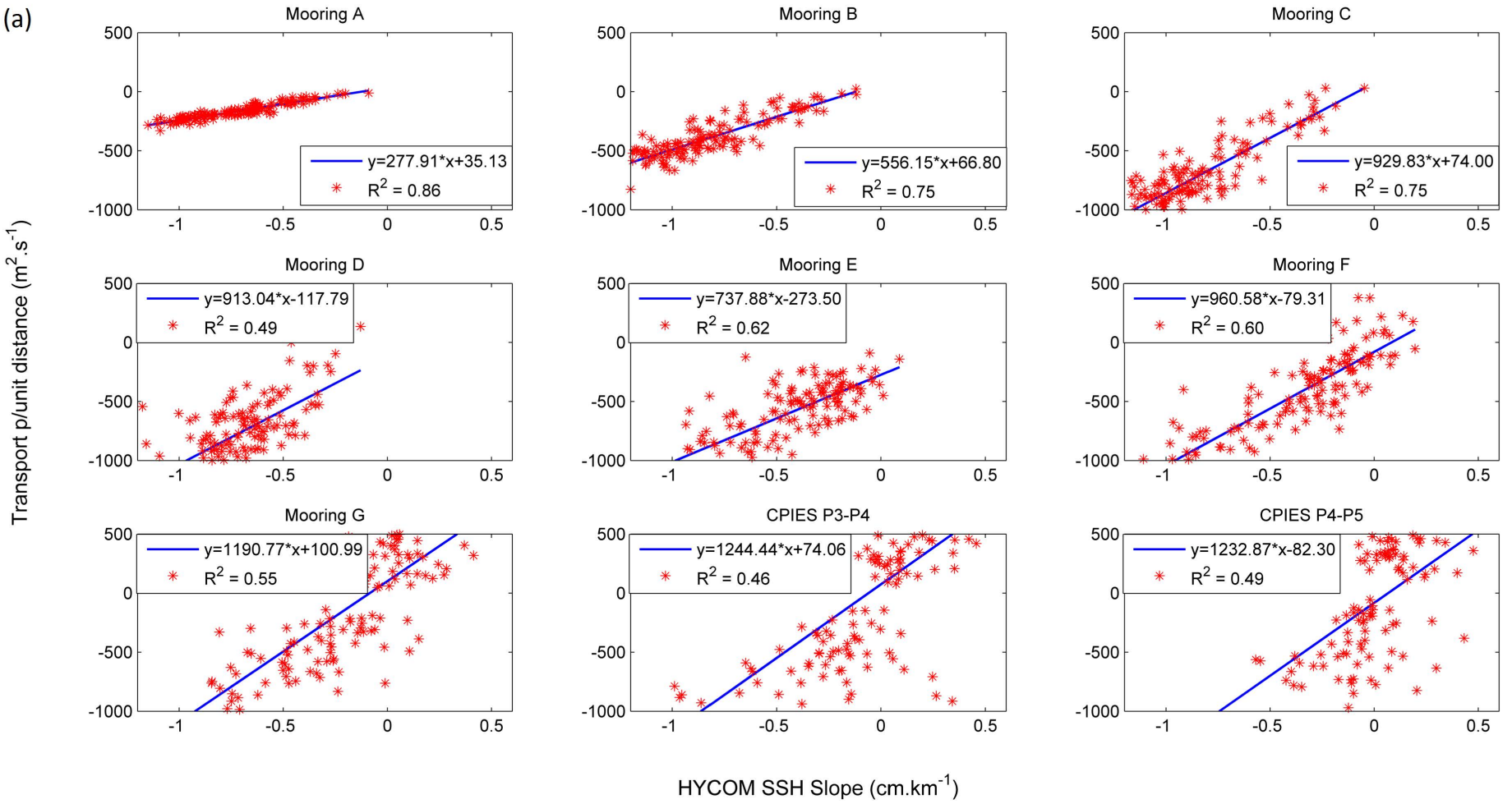

Figure A.3: Linear regression models showing the relationship between HYCOM SSH slope and transport per unit distance for T_{net}. Linear relationships were significant at 95% confidence interval (P-values $< 10^{-3}$).

Figure A.4: Linear regression models showing the relationship between HYCOM SSH slope and transport per unit distance for T_{sw}. Linear relationships were significant at 95% confidence interval (P-values $< 10^{-3}$).